

Confining QCD Strings, Casimir Scaling, and a Euclidean Approach to High-Energy Scattering

A. I. Shoshi^{1,a}, F. D. Steffen^{1,b}, H. G. Dosch^{1,c}, and H. J. Pirner^{1,2,d}

¹*Institut für Theoretische Physik, Universität Heidelberg,
Philosophenweg 16 & 19, D-69120 Heidelberg, Germany*

²*Max-Planck-Institut für Kernphysik, Postfach 103980,
D-69029 Heidelberg, Germany*

Abstract

We compute the chromo-field distributions of static color-dipoles in the fundamental and adjoint representation of $SU(N_c)$ in the loop-loop correlation model and find Casimir scaling in agreement with recent lattice results. Our model combines perturbative gluon exchange with the non-perturbative stochastic vacuum model which leads to confinement of the color-charges in the dipole via a string of color-fields. We compute the energy stored in the confining string and use low-energy theorems to show consistency with the static quark-antiquark potential. We generalize Meggiolaro's analytic continuation from parton-parton to gauge-invariant dipole-dipole scattering and obtain a Euclidean approach to high-energy scattering that allows us in principle to calculate S -matrix elements directly in lattice simulations of QCD. We apply this approach and compute the S -matrix element for high-energy dipole-dipole scattering with the presented Euclidean loop-loop correlation model. The result confirms the analytic continuation of the gluon field strength correlator used in all earlier applications of the stochastic vacuum model to high-energy scattering.

Keywords: Casimir Scaling, Confining String, Flux Tube, High-Energy Scattering, Low-Energy Theorems, Static Potential, Stochastic Vacuum Model

PACS numbers: 11.15.-q, 11.15.Kc, 12.38.-t, 12.38.Aw,

^ashoshi@tphys.uni-heidelberg.de

^bFrank.D.Steffen@thphys.uni-heidelberg.de

^cH.G.Dosch@thphys.uni-heidelberg.de

^dpir@tphys.uni-heidelberg.de

Contents

| | | |
|----------|--|-----------|
| 1 | Introduction | 1 |
| 2 | The Loop-Loop Correlation Model | 3 |
| 2.1 | Vacuum Expectation Value of one Wegner-Wilson Loop | 4 |
| 2.2 | The Loop-Loop Correlation Function | 7 |
| 2.3 | Perturbative and Non-Perturbative QCD Components | 12 |
| 3 | Chromo-Field Distributions of Color-Dipoles | 16 |
| 4 | Low-Energy Theorems | 25 |
| 5 | Euclidean Approach to High-Energy Scattering | 28 |
| 6 | Conclusion | 36 |
| A | The Static Color-Dipole Potential | 39 |
| B | Loop and Minimal Surface Parametrizations | 44 |
| C | χ-Computations with Minimal Surfaces | 46 |

1 Introduction

The structure of the *QCD vacuum* is responsible for color confinement, spontaneous chiral symmetry breaking, and dynamical mass generation [1]. Hadronic reactions are expected to show further manifestations of a non-trivial QCD vacuum. It is indeed a key issue to unravel the effects of confinement and topologically non-trivial gauge field configurations (such as instantons) on such reactions [2]. Moreover, it would be a significant breakthrough to understand the size, growth, and behavior of the hadronic cross sections with increasing c.m. energy from the QCD Lagrangian.

Lattice QCD is the principal theoretical tool to study the QCD vacuum from first principles. Numerical simulations of QCD on Euclidean lattices give strong evidence for color confinement and spontaneous chiral symmetry breaking and describe dynamical mass generation from the QCD Lagrangian [3]. However, since lattice QCD is limited to the Euclidean formulation of QCD, it cannot be applied in Minkowski space-time to simulate high-energy reactions in which particles are inherently moving near the light-cone. Furthermore, it is hard to understand from numerical simulations the important QCD mechanisms that lead, for example, to color-confinement. Here (phenomenological) models that allow analytic calculations are important.

In this work we introduce the Euclidean version of the *loop-loop correlation model* (LLCM) which has been developed in Minkowski space-time to describe high-energy reactions of hadrons and photons [4] on the basis of a functional integral approach [5–9]. The central element in our approach is the gauge-invariant Wegner-Wilson loop [10, 11] and the considered physical quantities are obtained from the vacuum expectation value (VEV) of one Wegner-Wilson loop, $\langle W_r[C] \rangle$, and the correlation of two Wegner-Wilson loops, $\langle W_{r_1}[C_1] W_{r_2}[C_2] \rangle$. Here $r_{(i)}$ indicates the $SU(N_c)$ representation of the Wegner-Wilson loops which we keep as general as possible. We express $\langle W_r[C] \rangle$ and $\langle W_{r_1}[C_1] W_{r_2}[C_2] \rangle$ in terms of the gauge-invariant bilocal gluon field strength correlator integrated over *minimal surfaces* by using the non-Abelian Stokes theorem and a matrix cumulant expansion in the Gaussian approximation. We decompose the gluon field strength correlator into a perturbative and a non-perturbative component. The *stochastic vacuum model* (SVM) [12] is used for the non-perturbative low-frequency background field and *perturbative gluon exchange* for the additional high-frequency contributions. This combination allows us to describe long and short distance correlations in agreement with lattice calculations of the gluon field strength correlator [13, 14]. Moreover, it leads to a static quark-antiquark potential with color-Coulomb behavior for small and confining linear rise for large source separations. We calculate the static quark-antiquark potential with the LLCM parameters determined in fits to high-energy scattering

data [4] and find good agreement with lattice data. We thus have one model that describes both static hadronic properties and high-energy reactions of hadrons and photons in good agreement with experimental and lattice QCD data.

We apply the LLCM to compute the *chromo-electric fields* generated by a static color-dipole in the fundamental and adjoint representation of $SU(N_c)$. The non-perturbative SVM component describes the formation of a color-flux tube that confines the two color-sources in the dipole [15] while the perturbative component leads to color-Coulomb fields. We find *Casimir scaling* for both the perturbative and non-perturbative contributions to the chromo-electric fields. The mean squared radius of the confining QCD string is calculated as a function of the dipole size. Transverse and longitudinal energy density profiles are provided to study the interplay between perturbative and non-perturbative physics for different dipole sizes. The transition from perturbative to string behavior is found at source separations of about 0.5 fm in agreement with the recent results of Lüscher and Weisz [16].

The *low-energy theorems*, known in lattice QCD as Michael sum rules [17], relate the energy and action stored in the chromo-fields of a static color-dipole to the corresponding ground state energy. The Michael sum rules, however, are incomplete in their original form [17]. We present the complete energy and action sum rules [18–20] in continuum theory taking into account the contributions to the action sum rule found in [21] and the trace anomaly contribution to the energy sum rule [18]. Using these low-energy theorems, we compare the energy and action stored in the confining string with the confining part of the static quark-antiquark potential. This allows us to confirm consistency of the model results and to determine the values of the β -function and the strong coupling α_s at the renormalization scale at which the non-perturbative SVM component is working. Earlier investigations along these lines have been incomplete since only the contribution from the traceless part of the energy-momentum tensor has been considered in the energy sum rule.

To study the effect of the confining QCD string examined in Euclidean space-time on high-energy reactions in Minkowski space-time, an *analytic continuation* from Euclidean to Minkowski space-time is needed. For investigations of high-energy reactions in our Euclidean model, the gauge-invariant bilocal gluon field strength correlator can be analytically continued from Euclidean to Minkowski space-time. This analytic continuation has been introduced for applications of the SVM to high-energy reactions [7–9] and is used in our Minkowskian applications of the LLCM [4, 22, 23]. Recently, an alternative analytic continuation for parton-parton scattering has been established in the perturbative context by Meggiolaro [24]. This analytic continuation has already been used to access high-energy scattering from the supergravity side of the AdS/CFT correspondence [25], which requires a positive definite metric in the definition of the minimal surface [26], and to examine the effect of instantons

on high-energy scattering [27].

In this work we generalize Meggiolaro’s analytic continuation [24] from parton-parton to gauge-invariant *dipole-dipole scattering* such that S -matrix elements for high-energy reactions can be computed from configurations of Wegner-Wilson loops in Euclidean space-time and with *Euclidean* functional integrals. This shows how one can access high-energy reactions directly in lattice QCD. First attempts in this direction have already been carried out but only very few signals could be extracted, while most of the data was dominated by noise [28]. We apply this approach to compute the scattering of dipoles at high-energy in the Euclidean LLCM. We recover exactly the result derived with the analytic continuation of the gluon field strength correlator [4]. This confirms the analytic continuation used in all earlier applications of the stochastic vacuum model to high-energy scattering [7–9, 29–34] including the Minkowskian applications of the LLCM [4, 22, 23]. In fact, the obtained S -matrix element has already been used as the basis for a unified description of hadronic high-energy reactions [4], to study saturation effects in hadronic cross sections [4, 22], and to investigate manifestations of the confining QCD string in high-energy reactions of photons and hadrons [23].

The outline of the paper is as follows: In Sec. 2, the loop-loop correlation model is introduced in its Euclidean version and the general computations of $\langle W_r[C] \rangle$ and $\langle W_{r_1}[C_1] W_{r_2}[C_2] \rangle$ are presented. Based on these evaluations, we compute in Sec. 3 the chromo-field distributions of color-dipoles with emphasis on Casimir scaling and the interplay between perturbative color-Coulomb behavior and non-perturbative formation of the confining QCD string. In Sec. 4, low-energy theorems are discussed and used to show consistency of the model results and to determine the values of β and α_s at the renormalization scale at which the non-perturbative SVM component is working. In Sec. 5, the Euclidean approach to high-energy scattering is presented and applied to compute high-energy dipole-dipole scattering in our Euclidean model. In the Appendices, we show the model results for the static dipole potential, give explicit parametrizations of the loops and the minimal surfaces, and provide the detailed computations for the results in the main text.

2 The Loop-Loop Correlation Model

In this section the vacuum expectation value (VEV) of one Wegner-Wilson loop and the correlation of two Wegner-Wilson loops is computed for arbitrary loop geometries within a Gaussian approximation in the gluon field strengths. The results are applied in the following sections. We describe our model for the QCD vacuum in which the stochastic vacuum model (SVM) [12] is used for the non-perturbative low-frequency

background field (long-distance correlations) and perturbative gluon exchange for the additional high-frequency contributions (short-distance correlations).

2.1 Vacuum Expectation Value of one Wegner-Wilson Loop

A crucial quantity in gauge theories is the Wegner-Wilson loop operator [10, 11]

$$W_r[C] = \tilde{\text{Tr}}_r \mathcal{P} \exp \left[-ig \oint_C dZ_\mu \mathcal{G}_\mu^a(Z) t_r^a \right]. \quad (2.1)$$

Concentrating on $SU(N_c)$ Wegner-Wilson loops, where N_c is the number of colors, the subscript r indicates a representation of $SU(N_c)$, $\tilde{\text{Tr}}_r = \text{Tr}_r(\cdots)/\text{Tr} \mathbb{1}_r$ is the normalized trace in the corresponding color-space with unit element $\mathbb{1}_r$, g is the strong coupling, and $\mathcal{G}_\mu(Z) = \mathcal{G}_\mu^a(Z) t_r^a$ represents the gluon field with the $SU(N_c)$ group generators in the corresponding representation, t_r^a , that demand the path ordering indicated by \mathcal{P} on the closed path C in space-time. A distinguishing theoretical feature of the Wegner-Wilson loop is its invariance under local gauge transformations in color-space. Therefore, it is the basic object in lattice gauge theories [3, 10, 11] and has been considered as the fundamental building block for a gauge theory in terms of gauge invariant variables [35]. Phenomenologically, the Wegner-Wilson loop represents the phase factor associated to the propagation of a very massive color-source in the representation r of the gauge group $SU(N_c)$.

To compute the expectation value of a Wegner-Wilson loop (2.1) in the QCD vacuum

$$\langle W_r[C] \rangle_G = \langle \tilde{\text{Tr}}_r \mathcal{P} \exp \left[-ig \oint_C dZ_\mu \mathcal{G}_\mu^a(Z) t_r^a \right] \rangle_G, \quad (2.2)$$

we transform the line integral over the loop C into an integral over the surface S with $\partial S = C$ by applying the *non-Abelian Stokes' theorem* [36]

$$\langle W_r[C] \rangle_G = \langle \tilde{\text{Tr}}_r \mathcal{P}_S \exp \left[-i \frac{g}{2} \int_S d\sigma_{\mu\nu}(Z) \mathcal{G}_{\mu\nu}^a(O, Z; C_{ZO}) t_r^a \right] \rangle_G, \quad (2.3)$$

where \mathcal{P}_S indicates surface ordering and O is an arbitrary reference point on the surface S . In Eq. (2.3), the gluon field strength tensor, $\mathcal{G}_{\mu\nu}(Z) = \mathcal{G}_{\mu\nu}^a(Z) t^a$, is parallel transported to the reference point O along the path C_{ZO}

$$\mathcal{G}_{\mu\nu}(O, Z; C_{ZO}) = \Phi(O, Z; C_{ZO})^{-1} \mathcal{G}_{\mu\nu}(Z) \Phi(O, Z; C_{ZO}) \quad (2.4)$$

with the QCD Schwinger string

$$\Phi(O, Z; C_{ZO}) = \mathcal{P} \exp \left[-ig \int_{C_{ZO}} dZ_\mu \mathcal{G}_\mu^a(Z) t_r^a \right]. \quad (2.5)$$

The QCD vacuum expectation value $\langle \dots \rangle_G$ represents functional integrals in which the functional integration over the fermion fields has already been carried out as indicated by the subscript G [6]. The model we use for the QCD vacuum works in the *quenched approximation* that does not allow string breaking through dynamical quark-antiquark production.

Due to the linearity of the functional integral, $\langle \tilde{\text{Tr}}_r \dots \rangle = \tilde{\text{Tr}}_r \langle \dots \rangle$, we can write

$$\langle W_r[C] \rangle_G = \tilde{\text{Tr}}_r \left\langle \mathcal{P}_S \exp \left[-i \frac{g}{2} \int_S d\sigma_{\mu\nu}(Z) \mathcal{G}_{\mu\nu}^a(O, Z; C_{ZO}) t_r^a \right] \right\rangle_G . \quad (2.6)$$

For the evaluation of (2.6), a *matrix cumulant expansion* is used as explained in [6] (cf. also [37])

$$\begin{aligned} & \left\langle \mathcal{P}_S \exp \left[-i \frac{g}{2} \int_S d\sigma(Z) \mathcal{G}(O, Z; C_{ZO}) \right] \right\rangle_G \\ &= \exp \left[\sum_{n=1}^{\infty} \frac{1}{n!} \left(-i \frac{g}{2} \right)^n \int d\sigma(X_1) \cdots d\sigma(X_n) K_n(X_1, \dots, X_n) \right] , \end{aligned} \quad (2.7)$$

where space-time indices are suppressed to simplify notation. The cumulants K_n consist of expectation values of *ordered* products of the non-commuting matrices $\mathcal{G}(O, Z; C_{ZO})$. The leading matrix cumulants are

$$K_1(X) = \langle \mathcal{G}(O, X; C_X) \rangle_G, \quad (2.8)$$

$$\begin{aligned} K_2(X_1, X_2) &= \langle \mathcal{P}_S [\mathcal{G}(O, X_1; C_{X_1}) \mathcal{G}(O, X_2; C_{X_2})] \rangle_G \\ &\quad - \frac{1}{2} (\langle \mathcal{G}(O, X_1; C_{X_1}) \rangle_G \langle \mathcal{G}(O, X_2; C_{X_2}) \rangle_G + (1 \leftrightarrow 2)) . \end{aligned} \quad (2.9)$$

Since the vacuum does not prefer a specific color direction, K_1 vanishes and K_2 becomes

$$K_2(X_1, X_2) = \langle \mathcal{P}_S [\mathcal{G}(O, X_1; C_{X_1}) \mathcal{G}(O, X_2; C_{X_2})] \rangle_G . \quad (2.10)$$

Now, we approximate the functional integral associated with the expectation values $\langle \dots \rangle_G$ as a *Gaussian integral* in the gluon field strength. Consequently, the cumulants factorize into two-point field correlators such that all higher cumulants, K_n with $n > 2$, vanish⁵ and $\langle W_r[C] \rangle_G$ can be expressed in terms of K_2

$$\begin{aligned} \langle W_r[C] \rangle_G &= \tilde{\text{Tr}}_r \exp \left[-\frac{g^2}{8} \int_S d\sigma_{\mu\nu}(X_1) \int_S d\sigma_{\rho\sigma}(X_2) \right. \\ &\quad \left. \left\langle \mathcal{P}_S [\mathcal{G}_{\mu\nu}^a(O, X_1; C_{X_1O}) t_r^a \mathcal{G}_{\rho\sigma}^b(O, X_2; C_{X_2O}) t_r^b] \right\rangle_G \right] \end{aligned} \quad (2.11)$$

⁵We are going to use the cumulant expansion in the Gaussian approximation also for perturbative gluon exchange. Here certainly the higher cumulants are non-zero.

Due to the color-neutrality of the vacuum, the gauge-invariant bilocal gluon field strength correlator contains a δ -function in color-space,

$$\left\langle \frac{g^2}{4\pi^2} [\mathcal{G}_{\mu\nu}^a(O, X_1; C_{X_1O}) \mathcal{G}_{\rho\sigma}^b(O, X_2; C_{X_2O})] \right\rangle_G =: \frac{1}{4} \delta^{ab} F_{\mu\nu\rho\sigma}(X_1, X_2, O; C_{X_1O}, C_{X_2O}) \quad (2.12)$$

which makes the surface ordering \mathcal{P}_S in (2.11) irrelevant. The tensor $F_{\mu\nu\rho\sigma}$ will be specified in Sec. 2.3. With (2.12) and the quadratic Casimir operator $C_2(r)$,

$$t_r^a t_r^a = t_r^2 = C_2(r) \mathbb{1}_r, \quad (2.13)$$

Eq. (2.11) reads

$$\left\langle W_r[C] \right\rangle_G = \tilde{\text{Tr}}_r \exp \left[-\frac{C_2(r)}{2} \chi_{SS} \mathbb{1}_r \right] = \exp \left[-\frac{C_2(r)}{2} \chi_{SS} \right], \quad (2.14)$$

where

$$\chi_{SS} := \frac{\pi^2}{4} \int_S d\sigma_{\mu\nu}(X_1) \int_S d\sigma_{\rho\sigma}(X_2) F_{\mu\nu\rho\sigma}(X_1, X_2, O; C_{X_1O}, C_{X_2O}). \quad (2.15)$$

In this rather general result (2.14) obtained directly from the color-neutrality of the QCD vacuum and the Gaussian approximation in the gluon field strengths, the more detailed aspects of the QCD vacuum and the geometry of the considered Wegner-Wilson loop are encoded in the function χ_{SS} which is computed in Appendix C for the rectangular loop shown in Fig. 8.

In explicit computations we use for S the *minimal surface*, which is the planar surface spanned by the loop, $C = \partial S$, that leads to Wilson's area law [12]. The minimal surface is represented in the upcoming figures by the shaded areas (cf. Figs. 8 and 11). Of course, the results should not dependent on the surface choice. In our model this will be fulfilled for the perturbative and non-perturbative non-confining component but not for the non-perturbative confining component in $F_{\mu\nu\rho\sigma}$ due to the Gaussian approximation and the associated truncation of the cumulant expansion. Nevertheless, since our results for the VEV of a rectangular Wegner-Wilson loop lead to a static quark-antiquark potential that is in good agreement with lattice data (see Appendix A), we are led to conclude that the choice of the minimal surface is required by the Gaussian approximation in the gluon field strengths. The minimal surface is also favored by other complementary approaches such as the strong coupling expansion in lattice QCD, where plaquettes cover the minimal surface, or large- N_c investigations, where the planar gluon diagrams dominate in the large- N_c limit. Within bosonic string theory, our minimal surface represents the world-sheet of the *rigid* string: Our model does not describe fluctuations or excitations of the string and thus cannot reproduce the Lüscher term which has recently been confirmed with unprecedented precision by Lüscher and Weisz [16].

2.2 The Loop-Loop Correlation Function

The computation of the *loop-loop correlation function* $\langle W_{r_1}[C_1]W_{r_2}[C_2] \rangle_G$ starts again with the application of the *non-Abelian Stokes' theorem* [36] that allows us to transform the line integrals over the loops $C_{1,2}$ into integrals over surfaces $S_{1,2}$ with $\partial S_{1,2} = C_{1,2}$

$$\begin{aligned} \left\langle W_{r_1}[C_1]W_{r_2}[C_2] \right\rangle_G &= \left\langle \tilde{\text{Tr}}_{r_1} \mathcal{P}_S \exp \left[-i \frac{g}{2} \int_{S_1} d\sigma_{\mu\nu}(X_1) \mathcal{G}_{\mu\nu}^a(O_1, X_1; C_{X_1 O_1}) t_{r_1}^a \right] \right. \\ &\quad \times \tilde{\text{Tr}}_{r_2} \mathcal{P}_S \exp \left[-i \frac{g}{2} \int_{S_2} d\sigma_{\rho\sigma}(X_2) \mathcal{G}_{\rho\sigma}^b(O_2, X_2; C_{X_2 O_2}) t_{r_2}^b \right] \left. \right\rangle_G \end{aligned} \quad (2.16)$$

where O_1 and O_2 are the reference points on the surfaces S_1 and S_2 , respectively, that enter through the non-Abelian Stokes' theorem. In order to ensure gauge invariance in our model, the gluon field strengths associated with the loops must be compared at *one* reference point O . Due to this physical constraint, the surfaces S_1 and S_2 are required to touch at a common reference point $O_1 = O_2 = O$.

To treat the product of the two traces in (2.16), we transfer the approach of Berger and Nachtmann [31], cf. also [4], to Euclidean space-time. Accordingly, the product of the two traces, $\tilde{\text{Tr}}_{r_1}(\cdots) \tilde{\text{Tr}}_{r_2}(\cdots)$, over $SU(N_c)$ matrices in the r_1 and r_2 representation, respectively, is interpreted as one trace $\tilde{\text{Tr}}_{r_1 \otimes r_2}(\cdots) := \text{Tr}_{r_1 \otimes r_2}(\cdots) / \text{Tr}_{r_1 \otimes r_2}(\mathbb{1}_{r_1 \otimes r_2})$ that acts in the tensor product space built from the r_1 and r_2 representations

$$\begin{aligned} \left\langle W_{r_1}[C_1]W_{r_2}[C_2] \right\rangle_G &= \left\langle \tilde{\text{Tr}}_{r_1 \otimes r_2} \left\{ \left[\mathcal{P}_S \exp \left[-i \frac{g}{2} \int_{S_1} d\sigma_{\mu\nu}(X_1) \mathcal{G}_{\mu\nu}^a(O, X_1; C_{X_1 O}) t_{r_1}^a \right] \otimes \mathbb{1}_{r_2} \right] \right. \right. \\ &\quad \times \left. \left. \left[\mathbb{1}_{r_1} \otimes \mathcal{P}_S \exp \left[-i \frac{g}{2} \int_{S_2} d\sigma_{\rho\sigma}(X_2) \mathcal{G}_{\rho\sigma}^b(O, X_2; C_{X_2 O}) t_{r_2}^b \right] \right] \right\} \right\rangle_G \end{aligned} \quad (2.17)$$

With the identities

$$\exp(t_{r_1}^a) \otimes \mathbb{1}_{r_2} = \exp(t_{r_1}^a \otimes \mathbb{1}_{r_2}) \quad (2.18)$$

$$\mathbb{1}_{r_1} \otimes \exp(t_{r_2}^a) = \exp(\mathbb{1}_{r_1} \otimes t_{r_2}^a) \quad (2.19)$$

the tensor products can be shifted into the exponents. Using the matrix multiplication relations in the tensor product space

$$\begin{aligned} (t_{r_1}^a \otimes \mathbb{1}_{r_2})(t_{r_1}^b \otimes \mathbb{1}_{r_2}) &= t_{r_1}^a t_{r_1}^b \otimes \mathbb{1}_{r_2} \\ (t_{r_1}^a \otimes \mathbb{1}_{r_2})(\mathbb{1}_{r_1} \otimes t_{r_2}^b) &= t_{r_1}^a \otimes t_{r_2}^b \end{aligned} \quad (2.20)$$

and the vanishing of the commutator

$$[t_{r_1}^a \otimes \mathbb{1}_{r_2}, \mathbb{1}_{r_1} \otimes t_{r_2}^b] = 0, \quad (2.21)$$

the two exponentials in (2.17) commute and can be written as one exponential

$$\left\langle W[C_1]W[C_2] \right\rangle_G = \left\langle \tilde{\text{Tr}}_{r_1 \otimes r_2} \mathcal{P}_S \exp \left[-i \frac{g}{2} \int_S d\sigma_{\mu\nu}(X) \hat{\mathcal{G}}_{\mu\nu}(O, X; C_{XO}) \right] \right\rangle_G \quad (2.22)$$

with the following gluon field strength tensor acting in the tensor product space

$$\hat{\mathcal{G}}_{\mu\nu}(O, X; C_{XO}) := \begin{cases} \mathcal{G}_{\mu\nu}^a(O, X; C_{XO})(t_{r_1}^a \otimes \mathbb{1}_{r_2}) & \text{for } X \in S_1 \\ \mathcal{G}_{\mu\nu}^a(O, X; C_{XO})(\mathbb{1}_{r_1} \otimes t_{r_2}^a) & \text{for } X \in S_2 \end{cases} \quad (2.23)$$

In Eq. (2.22) the surface integrals over S_1 and S_2 are written as one integral over the combined surface $S = S_1 + S_2$ so that the left-hand side (lhs) of (2.22) becomes very similar to the lhs of (2.3). This allows us to proceed analogously to the computation of $\langle W_r[C] \rangle_G$ in the previous section. After exploiting the linearity of the functional integral, the matrix cumulant expansion is applied, which holds for $\hat{\mathcal{G}}_{\mu\nu}(O, X; C_{XO})$ as well. Then, with the color-neutrality of the vacuum and by imposing the Gaussian approximation now in the color components of the gluon field strength tensor, only the $n = 2$ term of the matrix cumulant expansion survives, which leads to

$$\begin{aligned} & \left\langle W_{r_1}[C_1]W_{r_2}[C_2] \right\rangle_G \\ &= \tilde{\text{Tr}}_{r_1 \otimes r_2} \exp \left[-\frac{g^2}{8} \int_S d\sigma_{\mu\nu}(X_1) \int_S d\sigma_{\rho\sigma}(X_2) \left\langle \mathcal{P}_S [\hat{\mathcal{G}}_{\mu\nu}(O, X_1; C_{X_1O}) \hat{\mathcal{G}}_{\rho\sigma}(O, X_2; C_{X_2O})] \right\rangle_G \right] \end{aligned} \quad (2.24)$$

Note that the Gaussian approximation on the level of the color components of the gluon field strength tensor (component factorization) differs from the one on the level of the gluon field strength tensor (matrix factorization) used to compute $\langle W_r[C] \rangle$ in the original version of the SVM [12]. Nevertheless, with the additional ordering rule [15] explained in detail in Sec. 2.4 of [38], a modified component factorization is obtained that leads to the same area law as the matrix factorization.

Using definition (2.23) and relations (2.20), we now redivide the exponent in (2.24) into integrals of the ordinary parallel transported gluon field strengths over the sep-

arate surfaces S_1 and S_2

$$\begin{aligned}
\left\langle W_{r_1}[C_1]W_{r_2}[C_2] \right\rangle_G &= \tilde{\text{Tr}}_{r_1 \otimes r_2} \exp \left[\right. \\
&- \frac{g^2}{8} \int_{S_1} d\sigma_{\mu\nu}(X_1) \int_{S_2} d\sigma_{\rho\sigma}(X_2) \mathcal{P}_S \left[\left\langle \mathcal{G}_{\mu\nu}^a(O, X_1; C_{X_1 O}) \mathcal{G}_{\rho\sigma}^b(O, X_2; C_{X_2 O}) \right\rangle_G (t_{r_1}^a \otimes t_{r_2}^b) \right] \\
&- \frac{g^2}{8} \int_{S_2} d\sigma_{\mu\nu}(X_1) \int_{S_1} d\sigma_{\rho\sigma}(X_2) \mathcal{P}_S \left[\left\langle \mathcal{G}_{\mu\nu}^a(O, X_1; C_{X_1 O}) \mathcal{G}_{\rho\sigma}^b(O, X_2; C_{X_2 O}) \right\rangle_G (t_{r_1}^a \otimes t_{r_2}^b) \right] \\
&- \frac{g^2}{8} \int_{S_1} d\sigma_{\mu\nu}(X_1) \int_{S_1} d\sigma_{\rho\sigma}(X_2) \mathcal{P}_S \left[\left\langle \mathcal{G}_{\mu\nu}^a(O, X_1; C_{X_1 O}) \mathcal{G}_{\rho\sigma}^b(O, X_2; C_{X_2 O}) \right\rangle_G (t_{r_1}^a t_{r_1}^b \otimes \mathbb{1}_{r_2}) \right] \\
&- \frac{g^2}{8} \int_{S_2} d\sigma_{\mu\nu}(X_1) \int_{S_2} d\sigma_{\rho\sigma}(X_2) \mathcal{P}_S \left[\left\langle \mathcal{G}_{\mu\nu}^a(O, X_1; C_{X_1 O}) \mathcal{G}_{\rho\sigma}^b(O, X_2; C_{X_2 O}) \right\rangle_G (\mathbb{1}_{r_1} \otimes t_{r_2}^a t_{r_2}^b) \right] \left. \right]
\end{aligned} \tag{2.25}$$

Here the surface ordering \mathcal{P}_S is again irrelevant due to the color-neutrality of the vacuum (2.12), and (2.25) becomes

$$\begin{aligned}
\left\langle W_{r_1}[C_1]W_{r_2}[C_2] \right\rangle_G &= \tilde{\text{Tr}}_{r_1 \otimes r_2} \exp \left[- \frac{\chi_{S_1 S_2} + \chi_{S_2 S_1}}{2} (t_{r_1}^a \otimes t_{r_2}^a) \right. \\
&\quad \left. - \frac{\chi_{S_1 S_1}}{2} (t_{r_1}^a t_{r_1}^a \otimes \mathbb{1}_{r_2}) - \frac{\chi_{S_2 S_2}}{2} (\mathbb{1}_{r_1} \otimes t_{r_2}^a t_{r_2}^a) \right]
\end{aligned} \tag{2.26}$$

with

$$\chi_{S_i S_j} := \frac{\pi^2}{4} \int_{S_i} d\sigma_{\mu\nu}(X_1) \int_{S_j} d\sigma_{\rho\sigma}(X_2) F_{\mu\nu\rho\sigma}(X_1, X_2, O; C_{X_1 O}, C_{X_2 O}) . \tag{2.27}$$

The symmetries in the tensor structure of $F_{\mu\nu\rho\sigma}$ — see Eqs. (2.42), (2.44), and (2.48) — lead to $\chi_{S_1 S_2} = \chi_{S_2 S_1}$. With the quadratic Casimir operator (2.13) our final Euclidean result for general $SU(N_c)$ representations r_1 and r_2 becomes⁶

$$\begin{aligned}
&\left\langle W_{r_1}[C_1]W_{r_2}[C_2] \right\rangle_G \\
&= \tilde{\text{Tr}}_{r_1 \otimes r_2} \exp \left[- \chi_{S_1 S_2} (t_{r_1}^a \otimes t_{r_2}^a) - \left(\frac{C_2(r_1)}{2} \chi_{S_1 S_1} + \frac{C_2(r_2)}{2} \chi_{S_2 S_2} \right) \mathbb{1}_{r_1 \otimes r_2} \right]
\end{aligned} \tag{2.28}$$

where $\mathbb{1}_{r_1 \otimes r_2} := \mathbb{1}_{r_1} \otimes \mathbb{1}_{r_2}$. After specifying the representations r_1 and r_2 , the tensor product $t_{r_1 \otimes r_2} := t_{r_1}^a \otimes t_{r_2}^a$ can be expressed as a sum of projection operators P_i with the property $P_i t_{r_1 \otimes r_2} = \lambda_i P_i$

$$t_{r_1 \otimes r_2} = \sum \lambda_i P_i \quad \text{with} \quad \lambda_i = \frac{\tilde{\text{Tr}}_{r_1 \otimes r_2} (P_i t_{r_1 \otimes r_2})}{\tilde{\text{Tr}}_{r_1 \otimes r_2} (P_i)} , \tag{2.29}$$

⁶Note that the Euclidean $\chi_{S_i S_i} \neq 0$ in contrast to $\chi_{S_i S_i} = 0$ for Minkowskian light-like loops C_i considered in the original version of the Berger-Nachtmann approach [4, 31].

which corresponds to the decomposition of the tensor product space into irreducible representations.

For two Wegner-Wilson loops in the *fundamental representation* of $SU(N_c)$, $r_1 = r_2 = N_c$, that could describe the trajectories of two quark-antiquark pairs, the decomposition (2.29) becomes trivial

$$t_{N_c}^a \otimes t_{N_c}^a = \frac{N_c - 1}{2N_c} P_s - \frac{N_c + 1}{2N_c} P_a , \quad (2.30)$$

with the projection operators

$$(P_s)_{(\alpha_1 \alpha_2)(\beta_1 \beta_2)} = \frac{1}{2} (\delta_{\alpha_1 \beta_1} \delta_{\alpha_2 \beta_2} + \delta_{\alpha_1 \beta_2} \delta_{\alpha_2 \beta_1}) \quad (2.31)$$

$$(P_a)_{(\alpha_1 \alpha_2)(\beta_1 \beta_2)} = \frac{1}{2} (\delta_{\alpha_1 \beta_1} \delta_{\alpha_2 \beta_2} - \delta_{\alpha_1 \beta_2} \delta_{\alpha_2 \beta_1}) \quad (2.32)$$

that decompose the direct product space of two fundamental $SU(N_c)$ representations into the irreducible representations

$$N_c \otimes N_c = (N_c + 1)N_c/2 \oplus \overline{N_c(N_c - 1)/2} . \quad (2.33)$$

With $\text{Tr}_{N_c \otimes N_c} \mathbb{I}_{N_c \otimes N_c} = N_c^2$ and the projector properties

$$P_{s,a}^2 = P_{s,a} , \quad \text{Tr}_{N_c \otimes N_c} P_s = (N_c + 1)N_c/2 \quad \text{and} \quad \text{Tr}_{N_c \otimes N_c} P_a = (N_c - 1)N_c/2 \quad (2.34)$$

we find for the loop-loop correlation function with both loops in the fundamental $SU(N_c)$ representation

$$\begin{aligned} \left\langle W_{N_c}[C_1] W_{N_c}[C_2] \right\rangle_G &= \exp \left[-\frac{C_2(N_c)}{2} (\chi_{S_1 S_1} + \chi_{S_2 S_2}) \right] \\ &\times \left(\frac{N_c + 1}{2N_c} \exp \left[-\frac{N_c - 1}{2N_c} \chi_{S_1 S_2} \right] + \frac{N_c - 1}{2N_c} \exp \left[\frac{N_c + 1}{2N_c} \chi_{S_1 S_2} \right] \right) \end{aligned} \quad (2.35)$$

where

$$C_2(N_c) = \frac{N_c^2 - 1}{2N_c} . \quad (2.36)$$

For one Wegner-Wilson loop in the *fundamental* and one in the *adjoint representation* of $SU(N_c)$, $r_1 = N_c$ and $r_2 = N_c^2 - 1$, which is needed in Sec. 3 to investigate the chromo-field distributions around color-sources in the adjoint representation, the decomposition (2.29) reads

$$t_{N_c}^a \otimes t_{N_c^2 - 1}^a = -\frac{N_c}{2} P_1 + \frac{1}{2} P_2 - \frac{1}{2} P_3 \quad (2.37)$$

with the projection operators⁷ P_1 , P_2 , and P_3 that decompose the direct product space of one fundamental and one adjoint representation of $SU(N_c)$ into the irreducible representations

$$N_c \otimes N_c^2 - 1 = N_c \oplus \frac{1}{2} N_c(N_c - 1)(N_c + 2) \oplus \frac{1}{2} N_c(N_c + 1)(N_c - 2) \quad (2.38)$$

which reduces for $N_c = 3$ to the well-known $SU(3)$ decomposition

$$3 \otimes 8 = 3 \oplus 15 \oplus 6. \quad (2.39)$$

With $\text{Tr}_{N_c \otimes N_c^2 - 1} \mathbb{1}_{N_c \otimes N_c^2 - 1} = N_c(N_c^2 - 1)$ and projector properties analogous to (2.34), we obtain the loop-loop correlation function for one loop in the fundamental and one in the adjoint representation of $SU(N_c)$

$$\begin{aligned} \left\langle W_{N_c}[C_1] W_{N_c^2-1}[C_2] \right\rangle_G &= \exp \left[- \left(\frac{C_2(N_c)}{2} \chi_{S_1 S_1} + \frac{C_2(N_c^2-1)}{2} \chi_{S_2 S_2} \right) \right] \\ &\times \left(\frac{1}{N_c^2-1} \exp \left[\frac{N_c}{2} \chi_{S_1 S_2} \right] + \frac{N_c+2}{2(N_c+1)} \exp \left[-\frac{1}{2} \chi_{S_1 S_2} \right] + \frac{N_c-2}{2(N_c-1)} \exp \left[\frac{1}{2} \chi_{S_1 S_2} \right] \right) \end{aligned} \quad (2.40)$$

where

$$C_2(N_c^2-1) = N_c. \quad (2.41)$$

Note that our expressions for the loop-loop correlation function (2.29) and, more specifically, (2.35) and (2.40), are rather general results — as our result for the VEV of one Wegner-Wilson loop (2.14) — obtained directly from the color-neutrality of the QCD vacuum and the Gaussian approximation in the gluon field strengths. The loop geometries, which characterize the problem under investigation, are again encoded in the functions $\chi_{S_i S_j}$, where also more detailed aspects of the QCD vacuum enter in terms of $F_{\mu\nu\rho\sigma}$, i.e., the gauge-invariant bilocal gluon field strength correlator (2.12).

For the explicit computations of $\chi_{S_1 S_2}$ presented in Appendix C, one has to specify surfaces $S_{1,2}$ with the restriction $\partial S_{1,2} = C_{1,2}$ according to the non-Abelian Stokes' theorem. As illustrated in Figs. 1 and 7, we choose for $S_{1,2}$ the *minimal surfaces* that are built from the plane areas spanned by the corresponding loops $C_{1,2}$ and the infinitesimally thin tube which connects the two surfaces S_1 and S_2 . This is in line with our surface choice in applications of the LLCM to high-energy reactions [4, 22, 23] illustrated in Fig. 6. The thin tube allows us to compare the field strengths in surface S_1 with the field strengths in surface S_2 .

⁷The explicit form of the projection operators P_1 , P_2 , and P_3 can be found in [39] but note that we use the Gell-Mann (conventional) normalization of the gluons. The eigenvalues, λ_i , of the projection operators in (2.37) can be evaluated conveniently with the computer program “Colour” [40].

Due to the Gaussian approximation and the associated truncation of the cumulant expansion, the non-perturbative confining contribution to the loop-loop correlation function depends on the surface choice. Consequently, our results for the chromo-field distributions of color-dipoles obtained with the minimal surfaces (see Sec. 3) differ from the ones obtained with the pyramid mantle choice for the surfaces [15] even if the same parameters are used. With low-energy theorems we show in Sec. 4 that the minimal surfaces are actually required to ensure the consistency of our results for the VEV of one loop, $\langle W_r[C] \rangle$, and the loop-loop correlation function, $\langle W_{r_1}[C_1] W_{r_2}[C_2] \rangle$.

In applications of the model to high-energy scattering [4, 22, 23] the surfaces are interpreted as the world-sheets of the confining QCD strings in line with the picture obtained for the static dipole potential from the VEV of one loop. The minimal surfaces are the most natural choice to examine the scattering of two rigid strings without any fluctuations or excitations. Our model does unfortunately not choose the surface dynamically and, thus, cannot describe string flips between two non-perturbative color-dipoles. Recently, new developments towards a dynamical surface choice and a theory for the dynamics of the confining strings have been reported [41].

2.3 Perturbative and Non-Perturbative QCD Components

We decompose the gauge-invariant bilocal gluon field strength correlator (2.12) — as in the Minkowskian version of our model [4] — into a perturbative (P) and non-perturbative (NP) component

$$F_{\mu\nu\rho\sigma} = F_{\mu\nu\rho\sigma}^P + F_{\mu\nu\rho\sigma}^{NP} , \quad (2.42)$$

where $F_{\mu\nu\rho\sigma}^{NP}$ gives the low-frequency background field contribution modeled by the non-perturbative *stochastic vacuum model* (SVM) [12] and $F_{\mu\nu\rho\sigma}^P$ the additional high-frequency contribution described by *perturbative gluon exchange*. This combination allows us to describe long and short distance correlations in agreement with lattice calculations of the gluon field strength correlator [13, 14]. Moreover, this two component ansatz leads to the static quark-antiquark potential with color-Coulomb behavior for small and confining linear rise for large source separations in good agreement with lattice data as shown in Appendix A. Note that besides our two component ansatz an ongoing effort to reconcile the non-perturbative SVM with perturbative gluon exchange has led to complementary methods [41–43].

We compute the perturbative correlator $F_{\mu\nu\rho\sigma}^P$ from the gluon propagator in

Feynman-'t Hooft gauge

$$\left\langle \mathcal{G}_\mu^a(X_1) \mathcal{G}_\nu^b(X_2) \right\rangle = \int \frac{d^4 K}{(2\pi)^4} \frac{-i\delta^{ab}\delta_{\mu\nu}}{K^2 - m_G^2} e^{-iK(X_1 - X_2)} , \quad (2.43)$$

where we introduce an *effective gluon mass* of $m_G = m_\rho = 0.77 \text{ GeV}$ to limit the range of the perturbative interaction in the infrared (IR) region. This value is, of course, important for the interplay between the perturbative and non-perturbative component which comes out reasonable as illustrated in Appendix A for the static quark-antiquark potential. Moreover, it gives the “perturbative glueball” (GB) generated by our perturbative component a reasonable finite mass of $M_{GB}^P = 2m_G = 1.54 \text{ GeV}$.

In leading order in the strong coupling g , the resulting bilocal gluon field strength correlator is gauge-invariant already without the parallel transport to a common reference point so that $F_{\mu\nu\rho\sigma}^P$ depends only on the difference $Z = X_1 - X_2$

$$\begin{aligned} F_{\mu\nu\rho\sigma}^P(Z) &= \frac{g^2}{\pi^2} \frac{1}{2} \left[\frac{\partial}{\partial Z_\nu} (Z_\sigma \delta_{\mu\rho} - Z_\rho \delta_{\mu\sigma}) + \frac{\partial}{\partial Z_\mu} (Z_\rho \delta_{\nu\sigma} - Z_\sigma \delta_{\nu\rho}) \right] D_P(Z^2) \\ &= -\frac{g^2}{\pi^2} \int \frac{d^4 K}{(2\pi)^4} e^{-iKZ} \left[K_\nu K_\sigma \delta_{\mu\rho} - K_\nu K_\rho \delta_{\mu\sigma} + K_\mu K_\rho \delta_{\nu\sigma} - K_\mu K_\sigma \delta_{\nu\rho} \right] \tilde{D}'_P(K^2) \end{aligned} \quad (2.44)$$

with the perturbative correlation function

$$D_P(Z^2) = \frac{m_G^2}{2\pi^2 Z^2} K_2(m_G |Z|) \quad (2.45)$$

$$\tilde{D}'_P(K^2) := \frac{d}{dK^2} \int d^4 Z e^{iKZ} D_P(Z^2) = -\frac{1}{K^2 + m_G^2} . \quad (2.46)$$

The perturbative gluon field strength correlator has also been considered at next-to-leading order, where the dependence of the correlator on both the renormalization scale and the renormalization scheme becomes explicit and an additional tensor structure arises together with a path dependence of the correlator [44]. However, cancellations of contributions from this additional tensor structure have been shown [43]. We refer to Sec. 3.3 of [38] for a more detailed discussion of this issue.

We describe the perturbative correlations in our phenomenological applications only with the leading tensor structure (2.44) and take into account radiative corrections by replacing the constant coupling g^2 with the running coupling

$$g^2(Z^2) = 4\pi\alpha_s(Z^2) = \frac{48\pi^2}{(33 - 2N_f) \ln [(Z^{-2} + M^2)/\Lambda_{QCD}^2]} \quad (2.47)$$

in the final step of the computation of the χ -function, where the Euclidean distance $|Z|$ over which the correlation occurs provides the renormalization scale. In Eq. (2.47) N_f denotes the number of dynamical quark flavors, which is set to $N_f = 0$ in agreement with the quenched approximation, $\Lambda_{QCD} = 0.25$ GeV, and M allows us to freeze g^2 for $|Z| \rightarrow \infty$. Relying on low-energy theorems, we freeze the running coupling at the value $g^2 = 10.2$ ($\equiv \alpha_s = 0.81$), i.e., $M = 0.488$ GeV, at which our non-perturbative results for the confining potential and the total flux tube energy of a static quark-antiquark pair coincide (see Sec. 4).

The tensor structure (2.44) together with the perturbative correlation function (2.45) or (2.46) leads to the color-Yukawa potential (which reduces for $m_G = 0$ to the color-Coulomb potential) as shown in Appendix A. The perturbative contribution thus dominates the full potential at small quark-antiquark separations.

If the path connecting the points X_1 and X_2 is a straight line, the non-perturbative correlator $F_{\mu\nu\rho\sigma}^{NP}$ depends also only on the difference $Z = X_1 - X_2$. Then, the most general form of the correlator that respects translational, Lorentz, and parity invariance reads [12]

$$\begin{aligned}
F_{\mu\nu\rho\sigma}^{NP}(Z) &= F_{\mu\nu\rho\sigma}^{NPc}(Z) + F_{\mu\nu\rho\sigma}^{NPnc}(Z) \\
&= \frac{1}{3(N_c^2 - 1)} G_2 \left\{ \kappa (\delta_{\mu\rho}\delta_{\nu\sigma} - \delta_{\mu\sigma}\delta_{\nu\rho}) D(Z^2) \right. \\
&\quad \left. + (1 - \kappa) \frac{1}{2} \left[\frac{\partial}{\partial Z_\nu} (Z_\sigma\delta_{\mu\rho} - Z_\rho\delta_{\mu\sigma}) + \frac{\partial}{\partial Z_\mu} (Z_\rho\delta_{\nu\sigma} - Z_\sigma\delta_{\nu\rho}) \right] D_1(Z^2) \right\} \\
&= \frac{1}{3(N_c^2 - 1)} G_2 \int \frac{d^4 K}{(2\pi)^4} e^{-iKZ} \left\{ \kappa (\delta_{\mu\rho}\delta_{\nu\sigma} - \delta_{\mu\sigma}\delta_{\nu\rho}) \tilde{D}(K^2) \right. \\
&\quad \left. - (1 - \kappa) \left[K_\nu K_\sigma \delta_{\mu\rho} - K_\nu K_\rho \delta_{\mu\sigma} + K_\mu K_\rho \delta_{\nu\sigma} - K_\mu K_\sigma \delta_{\nu\rho} \right] \tilde{D}'_1(K^2) \right\} ,
\end{aligned} \tag{2.48}$$

where

$$\tilde{D}'_1(K^2) := \frac{d}{dK^2} \int d^4 Z D_1(Z^2) e^{iKZ} . \tag{2.49}$$

In all previous applications of the SVM, this form, depending only on $Z = X_1 - X_2$, has been used. New lattice results on the path dependence of the correlator [45] show a dominance of the shortest path. This result is effectively incorporated in the model since the straight paths dominate in the average over all paths.

The non-perturbative correlator (2.48) involves the gluon condensate $G_2 := \langle \frac{g^2}{4\pi^2} \mathcal{G}_{\mu\nu}^a(0) \mathcal{G}_{\mu\nu}^a(0) \rangle$ [46], the parameter κ that determines the non-Abelian character of the correlator, and the correlation length a that enters through the non-perturbative correlation functions D and D_1 .

We adopt for our calculations a simple *exponential correlation function*

$$D(Z^2) = D_1(Z^2) = \exp(-|Z|/a) , \quad (2.50)$$

which is motivated by lattice QCD measurements of the gluon field strength correlator [13, 14]. This correlation function stays positive for all Euclidean distances Z and, thus, is compatible with a spectral representation of the correlation function [47]. This means a conceptual improvement since the correlation function that has been used in several earlier applications of the SVM becomes negative at large distances [8, 15, 21, 29–32].

With the exponential correlation function (2.50) the lattice data of the gluon field strength correlator down to distances of 0.4 fm give the following values for the parameters of the non-perturbative correlator [14]: $G_2 = 0.173 \text{ GeV}^4$, $\kappa = 0.746$, and $a = 0.219 \text{ fm}$. We have optimized these parameters in a fit to high-energy scattering data [4]:

$$a = 0.302 \text{ fm}, \quad \kappa = 0.74, \quad G_2 = 0.074 \text{ GeV}^4 . \quad (2.51)$$

We use these optimized parameters (2.51) throughout this work. They lead to a static quark-antiquark potential that is in good agreement with lattice data (see Appendix A) and, in particular, give a QCD string tension (A.11) of $\sigma_3 = 0.22 \text{ GeV}^2 \equiv 1.12 \text{ GeV/fm}$ which is consistent with hadron spectroscopy [48], Regge theory [49], and lattice QCD investigations [50]. Moreover, the non-perturbative component with $a = 0.302 \text{ fm}$ generates a “non-perturbative glueball” with a mass of $M_{GB}^{NP} = 2/a = 1.31 \text{ GeV}$ which is smaller than $M_{GB}^P = 1.54 \text{ GeV}$ and thus governs the long-range correlations as expected. We thus have one model that describes both static hadronic properties and high-energy reactions of hadrons and photons in good agreement with experimental and lattice QCD data.

Finally, let us emphasize that the non-perturbative correlator (2.48) is a sum of the two different tensor structures, $F_{\mu\nu\rho\sigma}^{NP\,nc}$ and $F_{\mu\nu\rho\sigma}^{NP\,c}$, with characteristic behavior: The tensor structure $F_{\mu\nu\rho\sigma}^{NP\,nc}$ is characteristic for Abelian gauge theories, exhibits the same tensor structure as the perturbative correlator (2.44) and does not lead to confinement [12], i.e., it gives an exponentially vanishing static color-dipole potential at large dipole sizes as shown explicitly in Appendix A. In contrast, the tensor structure $F_{\mu\nu\rho\sigma}^{NP\,c}$ can only occur in non-Abelian gauge theories and Abelian gauge-theories with monopoles. It leads in the case of $\kappa \neq 0$ to confinement [12], i.e., to the confining linear increase of the static potential at large dipole sizes as demonstrated in Appendix A. Therefore, we call the tensor structure multiplied by $(1 - \kappa)$ non-confining (*nc*) and the one multiplied by κ confining (*c*).

3 Chromo-Field Distributions of Color-Dipoles

In this section we compute the chromo-electric fields generated by a static color-dipole in the fundamental and adjoint representation of $SU(N_c)$. We find formation of a color-flux tube that confines the two color-sources in the dipole. This confining string is analysed quantitatively. Its mean squared radius is calculated and transverse and longitudinal energy density profiles are provided. The interplay between perturbative and non-perturbative contributions to the chromo-field distributions is investigated and exact Casimir scaling is found for both contributions.

The static color-dipole — two static color-sources separated by a distance R in a net color-singlet state — is described by a Wegner-Wilson loop $W_r[C]$ with a rectangular path C of spatial extension R and temporal extension $T \rightarrow \infty$ (cf. Fig. 8) where r indicates the $SU(N_c)$ representation of the considered sources. A second small quadratic loop or plaquette in the fundamental representation placed at the space-time point X with side length $R_P \rightarrow 0$ and oriented along the $\alpha\beta$ -axes

$$P_{N_c}^{\alpha\beta}(X) = \tilde{\text{Tr}}_{N_c} \exp \left[-ig \oint_{C_P} dZ_\mu \mathcal{G}_\mu^a(Z) t_{N_c}^a \right] = 1 - R_P^4 \frac{g^2}{4N_c} \mathcal{G}_{\alpha\beta}^a(X) \mathcal{G}_{\alpha\beta}^a(X) + \mathcal{O}(R_P^6) \quad (3.1)$$

is needed — as a “Hall probe” — to calculate the chromo-field distributions at the space-time point X caused by the static sources [51, 52]

$$\Delta G_{r\alpha\beta}^2(X) := \left\langle \frac{g^2}{4\pi^2} \mathcal{G}_{\alpha\beta}^a(X) \mathcal{G}_{\alpha\beta}^a(X) \right\rangle_{W_r[C]} - \left\langle \frac{g^2}{4\pi^2} \mathcal{G}_{\alpha\beta}^a(X) \mathcal{G}_{\alpha\beta}^a(X) \right\rangle_{\text{vac}} \quad (3.2)$$

$$= - \lim_{R_P \rightarrow 0} \frac{1}{R_P^4} \frac{N_c}{\pi^2} \left[\frac{\langle W_r[C] P_{N_c}^{\alpha\beta}(X) \rangle}{\langle W_r[C] \rangle} - \langle P_{N_c}^{\alpha\beta}(X) \rangle \right] \quad (3.3)$$

with *no* summation over α and β in (3.1), (3.2), and (3.3). In definition (3.2) $\langle \dots \rangle_{W_r[C]}$ indicates the VEV in the presence of the static color-dipole while $\langle \dots \rangle_{\text{vac}}$ indicates the VEV in the absence of any color-sources. Depending on the plaquette orientation indicated by α and β , one obtains from (3.3) the squared components of the chromo-electric and chromo-magnetic field at the space-time point X

$$\Delta G_{r\alpha\beta}^2(X) = \frac{g^2}{4\pi^2} \begin{pmatrix} 0 & B_z^2 & B_y^2 & E_x^2 \\ B_z^2 & 0 & B_x^2 & E_y^2 \\ B_y^2 & B_x^2 & 0 & E_z^2 \\ E_x^2 & E_y^2 & E_z^2 & 0 \end{pmatrix} (X), \quad (3.4)$$

i.e., space-time plaquettes ($\alpha\beta = i4$) measure chromo-electric fields and space-space plaquettes ($\alpha\beta = ij$) chromo-magnetic fields. As shown in Fig. 1, we place the static

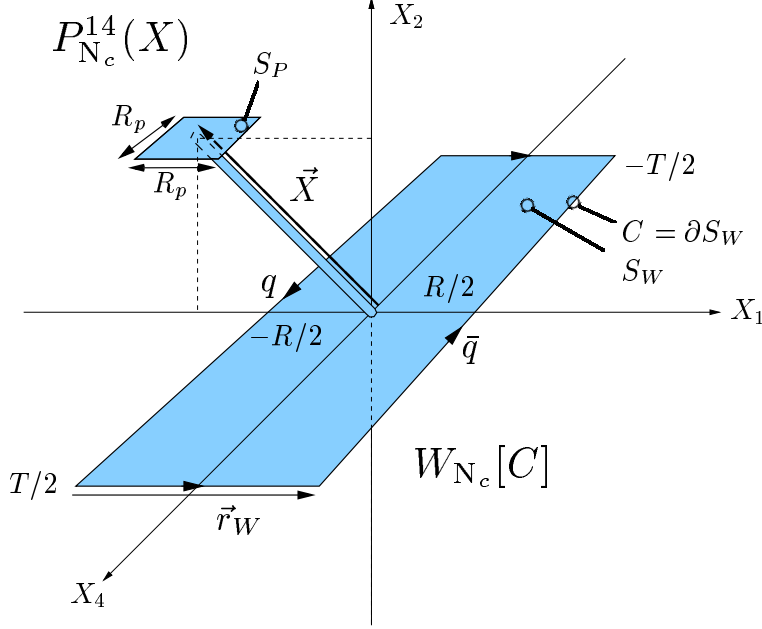


Figure 1: The plaquette-loop geometry needed to compute the squared chromo-electric field $E_{\parallel}^2(X)$ generated by a static color-dipole in the fundamental $SU(N_c)$ representation ($r = N_c$). The rectangular path C indicates the world-line of the static dipole described the Wegner-Wilson loop $W_{N_c}[C]$. The square with side length R_P illustrates the plaquette $P_{N_c}^{14}(X)$. The shaded areas represent the minimal surfaces used in our computation of the chromo-field distributions. The thin tube allows to compare the field strengths in surface S_P with the field strengths in surface S_W .

color-sources on the X_1 -axis at $(X_1 = \pm R/2, 0, 0, X_4)$ and use the following notation plausible from symmetry arguments

$$E_{\parallel}^2 = E_x^2, \quad E_{\perp}^2 = E_y^2 = E_z^2, \quad B_{\parallel}^2 = B_x^2, \quad B_{\perp}^2 = B_y^2 = B_z^2. \quad (3.5)$$

Figure 1 illustrates also the plaquette $P_{N_c}^{14}(X)$ at $X = (X_1, X_2, 0, 0)$ needed to compute $E_{\parallel}^2(X)$. Due to symmetry arguments, the complete information on the chromo-field distributions is obtained from plaquettes in “transverse” space $X = (X_1, X_2, 0, 0)$ with four different orientations, $\alpha\beta = 14, 24, 13, 23$, cf. (3.5).

The *energy* and *action density distributions* around a static color-dipole in the $SU(N_c)$ representation r are given by the squared chromo-field distributions

$$\varepsilon_r(X) = \frac{1}{2} \left(-\vec{E}^2(X) + \vec{B}^2(X) \right) \quad (3.6)$$

$$s_r(X) = -\frac{1}{2} \left(\vec{E}^2(X) + \vec{B}^2(X) \right) \quad (3.7)$$

with signs according to Euclidean space-time conventions. Low-energy theorems that relate the energy and action stored in the chromo-fields of the static color-dipole to the corresponding ground state energy are discussed in the next section.

For the chromo-field distributions of a static color-dipole in the *fundamental* representation of $SU(N_c)$, i.e., a static quark-antiquark pair, we obtain with our results for the VEV of one loop (2.14) and the correlation of two loops in the fundamental representation (2.35)

$$\begin{aligned} \Delta G_{N_c \alpha\beta}^2(X) = & - \lim_{R_P \rightarrow 0} \frac{1}{R_P^4} \frac{N_c}{\pi^2} \exp \left[-\frac{C_2(N_c)}{2} \chi_{S_P S_P} \right] \\ & \times \left(\frac{N_c + 1}{2N_c} \exp \left[-\frac{N_c - 1}{2N_c} \chi_{S_P S_W} \right] + \frac{N_c - 1}{2N_c} \exp \left[\frac{N_c + 1}{2N_c} \chi_{S_P S_W} \right] - 1 \right) \end{aligned} \quad (3.8)$$

where $\chi_{S_i S_j}$ is defined in (2.27). The subscripts P and W indicate surface integrations to be performed over the surfaces spanned by the plaquette and the Wegner-Wilson-loop, respectively. Choosing the surfaces — as illustrated by the shaded areas in Fig. 1 — to be the minimal surfaces connected by an infinitesimal thin tube (which gives no contribution to the integrals) it is clear that $\chi_{S_P S_P} \propto R_P^4$ and $\chi_{S_P S_W} \propto R_P^2$. Being interested in the chromo-fields at the space-time point X , the extension of the quadratic plaquette is taken to be infinitesimally small, $R_P \rightarrow 0$, so that one can expand the exponential functions and keep only the term of lowest order in R_P

$$\Delta G_{N_c \alpha\beta}^2(X) = -C_2(N_c) \lim_{R_P \rightarrow 0} \frac{1}{R_P^4} \frac{1}{4\pi^2} \chi_{S_P S_W}^2. \quad (3.9)$$

This result — obtained with the matrix cumulant expansion in very straightforward way — agrees exactly with the result derived in [15] with the expansion method. Indeed, the expansion method agrees for small χ -functions with the matrix cumulant expansion (Berger-Nachtmann approach) used in this work but breaks down for large χ -functions, where the matrix cumulant expansion is still applicable.

The chromo-field distributions of a static color-dipole in the *adjoint* representation of $SU(N_c)$, i.e., a static gluino pair, are computed analogously. Using our result (2.40) for the correlation of one loop in the fundamental representation (plaquette) with one loop in the adjoint representation (static sources), one obtains

$$\begin{aligned} \Delta G_{N_c-1 \alpha\beta}^2(X) = & - \lim_{R_P \rightarrow 0} \frac{1}{R_P^4} \frac{N_c}{\pi^2} \exp \left[-\frac{C_2(N_c)}{2} \chi_{S_P S_P} \right] \left(\frac{1}{N_c^2-1} \exp \left[\frac{N_c}{2} \chi_{S_P S_W} \right] \right. \\ & \left. + \frac{N_c+2}{2(N_c+1)} \exp \left[-\frac{1}{2} \chi_{S_P S_W} \right] + \frac{N_c-2}{2(N_c-1)} \exp \left[\frac{1}{2} \chi_{S_P S_W} \right] - 1 \right) \end{aligned} \quad (3.10)$$

which reduces — as explained for sources in the fundamental representation — to

$$\Delta G_{N_c^2-1\alpha\beta}^2(X) = -C_2(N_c^2-1) \lim_{R_P \rightarrow 0} \frac{1}{R_P^4} \frac{1}{4\pi^2} \chi_{S_P S_W}^2. \quad (3.11)$$

Thus, the squared chromo-electric fields of an adjoint dipole differ from those of a fundamental dipole only in the eigenvalue of the corresponding quadratic Casimir operator $C_2(r)$. In fact, *Casimir scaling* of the chromo-field distributions holds for dipoles in any representation r of $SU(N_c)$ in our model. As can be seen with the low-energy theorems discussed below, this is in line with the Casimir scaling of the static dipole potential — illustrated explicitly in Appendix A — that emerges trivially in our approach as a consequence of the Gaussian approximation used to truncate the cumulant expansion (2.7). Indeed, Casimir scaling hypothesis [53] has been verified to high accuracy for $SU(3)$ on the lattice [54, 55] which has been interpreted as a strong hint towards Gaussian dominance in the QCD vacuum and, thus, as evidence for a strong suppression of higher cumulant contributions [56, 57]. Also the Casimir scaling of the chromo-field distributions has been considered on the lattice for $SU(2)$ where only slight deviations have been found that were interpreted as hints towards adjoint quark screening [58].

The shape of the field distributions around the color-dipole is identical for all $SU(N_c)$ representations r and given by $\chi_{S_P S_W}^2$. This illustrates clearly a shortcoming of our model. Working in the quenched approximation, one expects a difference between fundamental and adjoint dipoles: *string breaking* cannot occur in fundamental dipoles as dynamical quark-antiquark production is excluded but should be present for adjoint dipoles because of gluonic vacuum polarization. Comparing (3.9) with (3.11) it is clear that this difference is not described in our model. In fact, as shown in Appendix A, string breaking is neither described for fundamental nor for adjoint dipoles. Interestingly, even on the lattice there has been no striking evidence for adjoint quark screening in quenched QCD [59]. It is even conjectured that the Wegner-Wilson loop operator is not suited to studies of string breaking [60].

In the LLCM there are perturbative (P) and non-perturbative (NP) contributions to the chromo-electric fields according to the structure of the gluon field strength correlator, (2.12) and (2.42),

$$\begin{aligned} \Delta G_{r\alpha\beta}^2(X) = & -C_2(r) \lim_{R_P \rightarrow 0} \frac{1}{R_P^4} \frac{1}{\pi^2} \\ & \times \left\{ (\chi_{S_P S_W}^P(X))_{\alpha\beta}^2 + \left[(\chi_{S_P S_W}^{NP\,nc}(X))_{\alpha\beta} + (\chi_{S_P S_W}^{NP\,c}(X))_{\alpha\beta} \right]^2 \right\} \end{aligned} \quad (3.12)$$

where we have demanded the non-interference of perturbative and non-perturbative correlations in line with previous applications of our model [4, 22, 23]. In the follow-

ing we give only the final results of the χ -functions for the minimal surfaces shown in Fig. 1. Details on their derivation can be found in Appendix C.

The *perturbative contribution* (P) described by massive gluon exchange leads, of course, to the well-known *color-Yukawa field* that reduces to the *color-Coulomb field* for $m_g = 0$. It contributes only to the color-electric fields, $E_{\parallel}^2 = E_x^2$ ($\alpha\beta = 14$) and $E_{\perp}^2 = E_y^2 = E_z^2$ ($\alpha\beta = 24$), and reads explicitly for $X = (X_1, X_2, 0, 0)$

$$(\chi_{S_P S_W}^P(X))_{14} = -\frac{R_P^2}{2} \int_{-\infty}^{\infty} d\tau \left\{ (X_1 - R/2) g^2(Z_{1A}^2) D_P(Z_{1A}^2) \right. \\ \left. - (X_1 + R/2) g^2(Z_{1C}^2) D_P(Z_{1C}^2) \right\} \quad (3.13)$$

$$(\chi_{S_P S_W}^P(X))_{24} = -\frac{R_P^2}{2} \int_{-\infty}^{\infty} d\tau X_2 \left\{ g^2(Z_{1A}^2) D_P(Z_{1A}^2) - g^2(Z_{1C}^2) D_P(Z_{1C}^2) \right\} \quad (3.14)$$

with the perturbative correlation function (2.45), the running coupling (2.47), and

$$Z_{1A}^2 = \left(X_1 - \frac{R}{2}\right)^2 + X_2^2 + \tau^2 \quad \text{and} \quad Z_{1C}^2 = \left(X_1 + \frac{R}{2}\right)^2 + X_2^2 + \tau^2. \quad (3.15)$$

The *non-confining non-perturbative contribution* ($NP nc$) has the same structure as the perturbative contribution — as expected from the identical tensor structure — but differs, of course, in the prefactors and the correlation function, $D_1 \neq D_P$. Its contributions to the color-electric fields $E_{\parallel}^2 = E_x^2$ ($\alpha\beta = 14$) and $E_{\perp}^2 = E_y^2 = E_z^2$ ($\alpha\beta = 24$) read for $X = (X_1, X_2, 0, 0)$

$$(\chi_{S_P S_W}^{NP nc}(X))_{14} = -\frac{R_P^2 \pi^2 G_2 (1-\kappa)}{6 (N_c^2 - 1)} \int_{-\infty}^{\infty} d\tau \left\{ (X_1 - R/2) D_1(Z_{1A}^2) \right. \\ \left. - (X_1 + R/2) D_1(Z_{1C}^2) \right\} \quad (3.16)$$

$$(\chi_{S_P S_W}^{NP nc}(X))_{24} = -\frac{R_P^2 \pi^2 G_2 (1-\kappa)}{6 (N_c^2 - 1)} \int_{-\infty}^{\infty} d\tau X_2 \left\{ D_1(Z_{1A}^2) - D_1(Z_{1C}^2) \right\} \quad (3.17)$$

with the exponential correlation function (2.50) and Z_{1A}^2 and Z_{1C}^2 as given in (3.15).

The *confining non-perturbative contribution* ($NP c$) has a different structure that leads to confinement and flux-tube formation. It gives only contributions to the chromo-electric field $E_{\parallel}^2 = E_x^2$ ($\alpha\beta = 14$) that read for $X = (X_1, X_2, 0, 0)$

$$(\chi_{S_P S_W}^{NP c}(X))_{14} = R_P^2 R \frac{\pi^2 G_2 \kappa}{3 (N_c^2 - 1)} \int_0^1 d\rho D^{(3)}(\vec{Z}_{\perp}^2), \quad (3.18)$$

with the correlation function

$$D^{(3)}(\vec{Z}^2) := \int \frac{d^4 K}{(2\pi)^3} e^{iKZ} \tilde{D}(K^2) \delta(K_4) = 2 |\vec{Z}| K_1[|\vec{Z}|/a], \quad (3.19)$$

derived from the exponential correlation function (2.50), and

$$\vec{Z}_\perp^2 = [X_1 + (1/2 - \rho)R]^2 + X_2^2 . \quad (3.20)$$

In our model, there are no contributions to the *chromo-magnetic fields*, i.e., the static color-charges do not affect the magnetic background field

$$B_\parallel^2 = B_x^2 = 0 \quad \text{and} \quad B_\perp^2 = B_y^2 = B_z^2 = 0 , \quad (3.21)$$

which can be seen from the corresponding plaquette-loop geometries as pointed out in Appendix C. Thus, the energy and action densities are identical in our approach and completely determined by the squared chromo-electric fields

$$\varepsilon_r(X) = s_r(X) = -\frac{1}{2} \vec{E}^2(X) . \quad (3.22)$$

This picture is in agreement with other effective theories of confinement such as the ‘t Hooft-Mandelstam picture [61] or dual QCD [62] and, indeed, a relation between the dual Abelian Higgs model and the SVM has been established [63]. In contrast, lattice investigations work at scales at which the chromo-electric and chromo-magnetic fields are of similar magnitude [20, 64]. Using low-energy theorems, we will see in the next section, that the vanishing of the chromo-magnetic fields determines the value of the β -function at the renormalization scale at which the non-perturbative component of our model is working.

The *longitudinal* and *transverse energy density profiles* generated by color-dipoles in the fundamental representation ($r = 3$) of $SU(N_c = 3)$ are shown for quark-antiquark separations (dipole sizes) of $R = 0.1, 0.5, 1$ and 1.5 fm in Figs. 2 and 3. The perturbative and non-perturbative contributions are given in the dotted and dashed lines, respectively, and the sum of both in the solid lines. The open and filled circles indicate the quark and antiquark positions. As can be seen from (3.3) and (3.4), we cannot compute the energy density separately but only the product $g^2 \varepsilon_r(X)$. Nevertheless, a comparison of the total energy stored in chromo-electric fields to the ground state energy of the color-dipole via low-energy theorems yields $g^2 = 10.2$ ($\equiv \alpha_s = 0.81$) for the non-perturbative SVM component as shown in the next section.

In Figs. 2 and 3 the formation of the confining string (flux tube) with increasing source separations R can be seen explicitly: For small dipoles, $R = 0.1$ fm, perturbative physics dominates and non-perturbative correlations are negligible. For large dipoles, $R \gtrsim 1$ fm, the non-perturbative correlations lead to formation of a narrow flux tube which dominates the chromo-electric fields between the color-sources.

Figure 4 shows the evolution of the transverse width (upper plot) and height

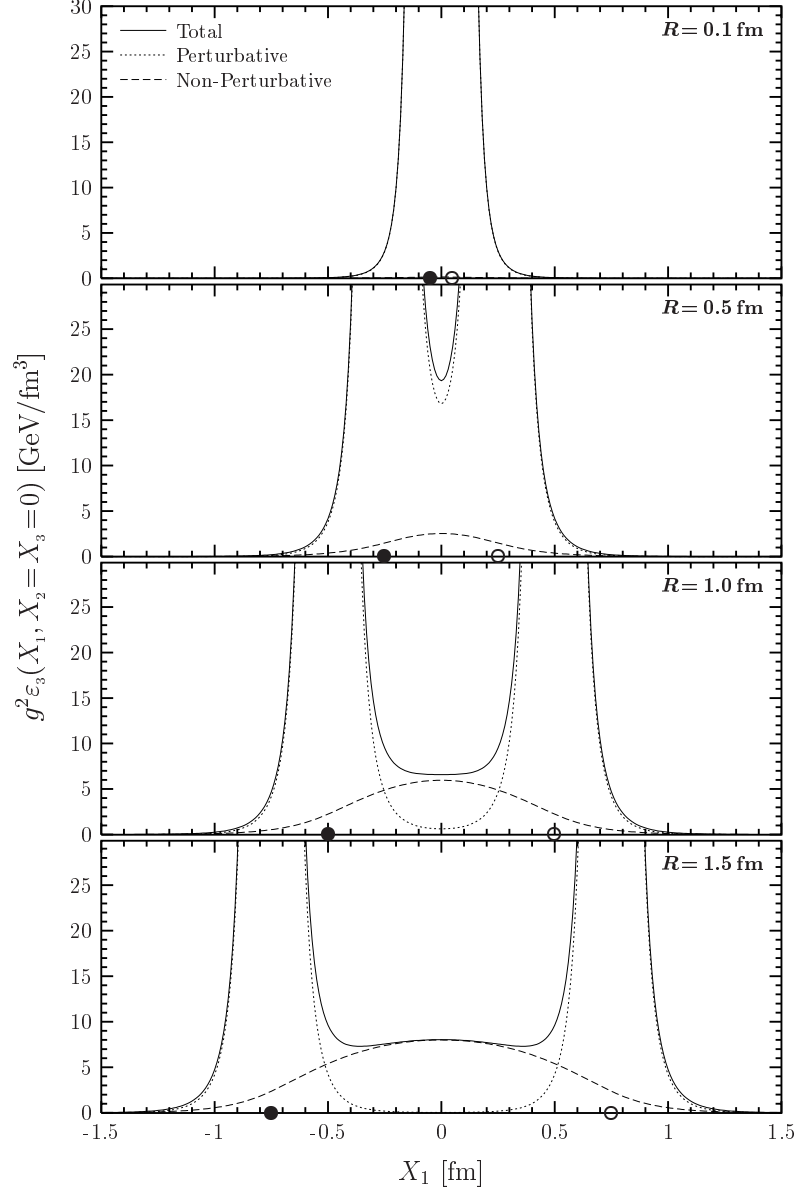


Figure 2: Longitudinal energy density profiles $g^2\epsilon_3(X_1, X_2=X_3=0)$ generated by color-dipoles in the fundamental $SU(3)$ representation ($r=3$) for quark-antiquark separations of $R = 0.1, 0.5, 1$ and 1.5 fm. The dotted and dashed lines give the perturbative and non-perturbative contributions and the solid lines the sum of both. The open and filled circles indicate the quark and antiquark positions. For small dipoles, $R = 0.1$ fm, perturbative physics dominates and non-perturbative correlations are negligible. For large dipoles, $R \gtrsim 1$ fm, the formation of the confining string (flux tube) can be seen which dominates the chromo-electric fields between the color-sources.

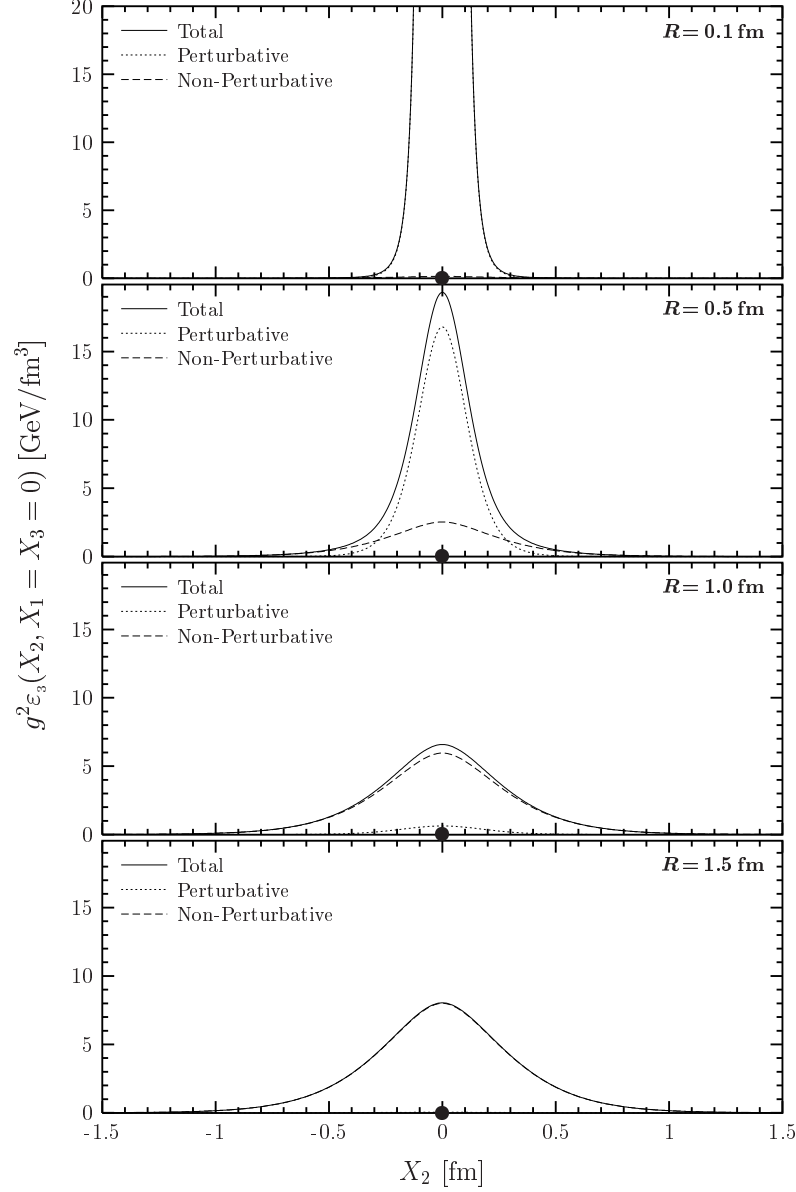


Figure 3: Transverse energy density profiles $g^2\epsilon_3(X_2, X_1 = X_3 = 0)$ of color-dipoles in the fundamental $SU(3)$ representation ($r = 3$) for quark-antiquark separations of $R = 0.1, 0.5, 1$ and 1.5 fm. The dotted and dashed lines give the perturbative and non-perturbative contributions and the solid lines the sum of both. The filled circles indicate the positions of the color-sources. For small dipoles, $R = 0.1$ fm, perturbative physics dominates and non-perturbative correlations are negligible. For large dipoles, $R \gtrsim 1$ fm, the formation the confining string (flux tube) can be seen which dominates the chromo-electric fields between the color-sources.

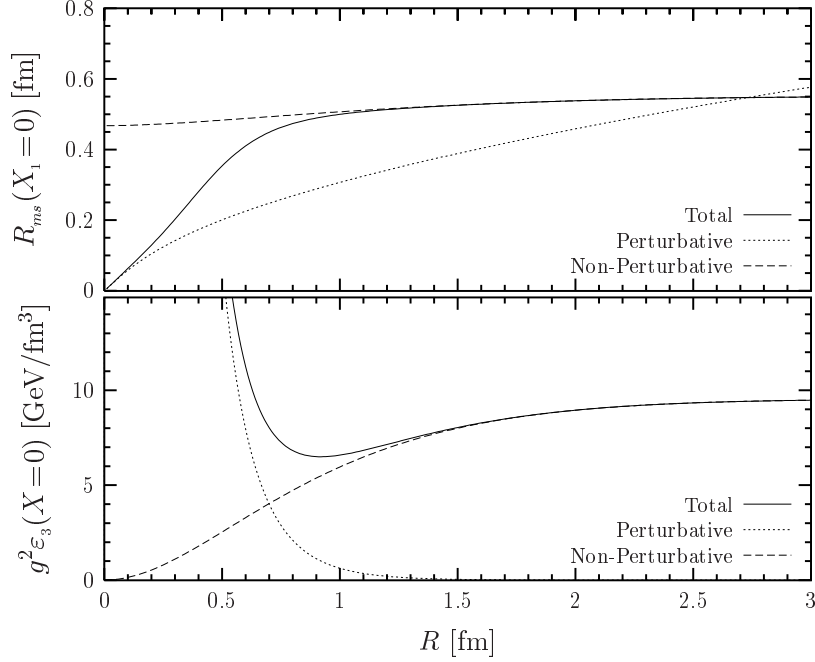


Figure 4: Root mean squared radius R_{ms} of the flux tube and energy density in the center of a fundamental $SU(3)$ dipole $g^2\epsilon_3(X=0)$ as a function of the dipole size R . Perturbative and non-perturbative contributions are given respectively in the dotted and dashed lines and the sum of both in the solid lines. For large R , both the width and height of the flux tube in the central region are governed completely by non-perturbative physics and saturate respectively at $R_{ms}^{R\rightarrow\infty} \approx 0.55$ fm and $\epsilon_3^{R\rightarrow\infty}(X=0) \approx 1$ GeV/fm³. The latter value is extracted with the result $g^2 = 10.2$ deduced from low-energy theorems in the next section.

(lower plot) of the flux tube in the central region of the Wegner-Wilson loop as a function of the dipole size R where perturbative and non-perturbative contributions are given in the dotted and dashed lines, respectively, and the sum of both in the solid lines. The width of the flux tube is best described by the root mean squared (ms) radius

$$R_{ms} = \sqrt{\frac{\int dX_{\perp} X_{\perp}^3 g^2\epsilon_r(X_1=0, X_{\perp})}{\int dX_{\perp} X_{\perp} g^2\epsilon_r(X_1=0, X_{\perp})}}, \quad (3.23)$$

which is universal for dipoles in all $SU(N_c)$ representations r as the Casimir factors divide out. The height of the flux tube is given by the energy density in the center of the considered dipole, $g^2\epsilon_r(X=0)$. For large source separations, $R \gtrsim 1$ fm, both the width and height of the flux tube in the central region of the Wegner-Wilson loop are governed completely by non-perturbative physics and saturate for a fundamental

$SU(3)$ dipole ($r = N_c = 3$) at reasonable values of

$$R_{ms}^{R \rightarrow \infty} \approx 0.55 \text{ fm} \quad \text{and} \quad \varepsilon_3^{R \rightarrow \infty}(X=0) \approx 1 \text{ GeV/fm}^3 \quad \text{with} \quad g^2 = 10.2 . \quad (3.24)$$

Note that the qualitative features of the non-perturbative SVM component do not depend on the specific choice for the parameters, surfaces, and correlation functions and have already been discussed with the pyramid mantle choice of the surface and different correlation functions in the first investigation of flux-tube formation in the SVM [15]. The quantitative results, however, are sensitive to the parameter values, the surface choice, and the correlation functions and are presented above for the first time with the LLCM parameters, the minimal surfaces, and the exponential correlation function.

4 Low-Energy Theorems

In this section we use low-energy theorems to test the consistency of the non-perturbative SVM component and to determine the value of the β -function and $\alpha_s = g^2/(4\pi)$ at the renormalization scale at which this component is working. The considered energy and action sum rules allow us to confirm the consistency of our loop-loop correlation result with the result obtained for the VEV of one loop.

Many low-energy theorems have been derived in continuum theory by Novikov, Shifman, Vainshtein, and Zakharov [65] and in lattice gauge theory by Michael [17]. Here, we consider the energy and action sum rules — known in lattice QCD as *Michael sum rules* — that relate the energy and action stored in the chromo-fields of a static color-dipole to the corresponding ground state energy [11, 66]

$$E_r(R) = - \lim_{T \rightarrow \infty} \frac{1}{T} \ln \langle W_r[C] \rangle . \quad (4.1)$$

In their original form [17], however, the Michael sum rules are incomplete [18, 21]. In particular, significant contributions to the energy sum rule from the trace anomaly of the energy-momentum tensor have been found [18] that modify the naively expected relation in line with the importance of the trace anomaly found for hadron masses [67]. Taking all these contributions into account, the *energy* and *action sum rule* read respectively [18–20]

$$E_r(R) = \int d^3X \varepsilon_r(X) - \frac{1}{2} \frac{\beta(g)}{g} \int d^3X s_r(X) \quad (4.2)$$

$$E_r(R) + R \frac{\partial E_r(R)}{\partial R} = - \frac{2\beta(g)}{g} \int d^3X s_r(X) \quad (4.3)$$

where $\beta(g) = \mu \partial g / \partial \mu$ with the renormalization scale μ . Inserting (4.3) into (4.2), we find the following relation between the total energy stored in the chromo-fields $E_r^{\text{tot}}(R)$ and the ground state energy $E_r(R)$

$$E_r^{\text{tot}}(R) := \int d^3X \varepsilon_r(X) = \frac{1}{4} \left(3 E_r(R) - R \frac{\partial E_r(R)}{\partial R} \right) . \quad (4.4)$$

The difference from the naive expectation that the full ground state energy of the static color-sources is stored in the chromo-fields is due to the trace anomaly contribution [18] described by the second term on the right-hand side (rhs) of (4.2).

With the low energy theorems (4.3) and (4.4) the ratio of the integrated squared chromo-magnetic to the integrated squared chromo-electric field distributions can be derived

$$Q(R) := \frac{\int d^3X \vec{B}^2(X)}{\int d^3X \vec{E}^2(X)} = \frac{(2 + 6 \beta(g)/g) E_r(R) + (1 - \beta(g)/g) R \frac{\partial E_r(R)}{\partial R}}{(2 - 6 \beta(g)/g) E_r(R) + (1 + \beta(g)/g) R \frac{\partial E_r(R)}{\partial R}} , \quad (4.5)$$

which becomes for $E_r(R) = \sigma_r R + E_{\text{self}}$ after subtraction of the self-energy contributions, i.e., the linear potential $V_r(R) = \sigma_r R$ with string tension σ_r in the considered representation r ,

$$Q(R) \Big|_{V_r(R)=\sigma_r R} = \frac{2 + \beta(g)/g}{2 - \beta(g)/g} . \quad (4.6)$$

In our model there are no contributions to the chromo-magnetic fields (3.21) so that — as already discussed in the previous section — the energy and action densities are identical and completely determined by the squared chromo-electric fields (3.22). Since the non-perturbative SVM component of our model describes the confining linear potential for large source separations R , this allows us to determine from (4.6) immediately the value of the β -function at the scale μ_{NP} at which the non-perturbative component is working

$$\frac{\beta(g)}{g} \Big|_{\mu=\mu_{NP}} = -2 . \quad (4.7)$$

Concentrating on the confining non-perturbative component (NPc) we now use (4.4) to determine the value of $\alpha_s = g^2/(4\pi)$ at which the non-perturbative SVM component is working. The rhs of (4.4) is obtained directly from the confining contribution to the static potential $E_r^{NPc}(R) = V_r^{NPc}(R)$ given in (A.7) in Appendix A. The lhs of (4.4), however, involves a division by the *a priori* unknown value of g^2 after integrating $g^2 \varepsilon_r(X)$ for the chromo-electric field of the confining non-perturbative component (3.18). As discussed in the previous section, we cannot compute the

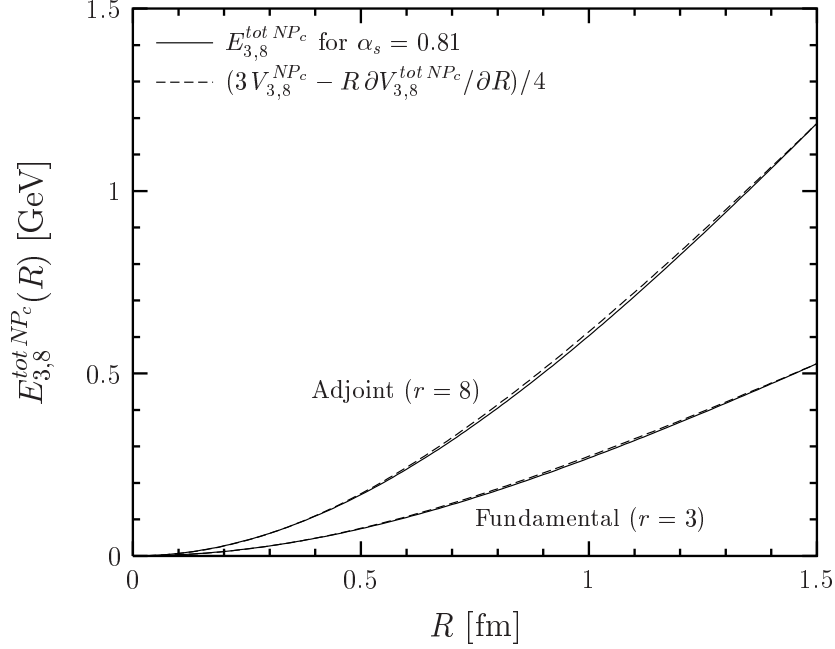


Figure 5: The total energy stored in the chromo-field distributions around a static color-dipole of size R in the fundamental ($r = 3$) and adjoint ($r = 8$) representation of $SU(3)$ from the confining non-perturbative SVM component, $E_{3,8}^{tot NP_c}(R)$, for $\alpha_s = 0.81$ (solid lines) compared with the relation to the corresponding ground state energy (dashed lines) given by the low-energy theorem (4.4). Good consistency is found even down to very small values of R .

energy density separately but only the product $g^2 \varepsilon_r(X)$. Adjusting the value of g^2 such that (4.4) is exactly fulfilled for source separations of $R = 1.5$ fm, we find that the non-perturbative component is working at the scale μ_{NP} at which

$$g^2(\mu_{NP}) = 10.2 \quad \equiv \quad \alpha_s(\mu_{NP}) = 0.81 . \quad (4.8)$$

As already mentioned in Sec. 2.3, we use this value as a practical asymptotic limit for the simple one-loop coupling (2.47) used in our perturbative component. Note that earlier SVM investigations along these lines have found a smaller value of $\alpha_s(\mu_{NP}) = 0.57$ with the pyramid mantle choice for the surface [15, 21] but were incomplete since only the contribution from the traceless part of the energy-momentum tensor has been considered in the energy sum rule.

In Fig. 5 we show the total energy stored in the chromo-field distributions around a static color-dipole in the fundamental ($r = 3$) and adjoint ($r = 8$) representation of $SU(3)$ from the confining non-perturbative SVM component, $E_{3,8}^{tot NP_c}(R)$, for $\alpha_s = 0.81$ (solid lines) as a function of the dipole size R . Comparing this total energy, which appears on the lhs of (4.4), with the corresponding rhs of (4.4) (dashed lines),

we find good consistency even down to very small values of R . This is a nontrivial and important result as it confirms the consistency of our loop-loop correlation result — needed to compute the chromo-electric field — with the result obtained for the VEV of one loop — needed to compute the static potential $V_r^{NP_c}(R)$. Moreover, it shows that the minimal surfaces ensure the consistency of our non-perturbative component. The good consistency found for the pyramid mantle choice of the surface relies on the naively expected energy sum rule [15, 21] in which the contribution from the traceless part of the energy-momentum tensor is not taken into account.

5 Euclidean Approach to High-Energy Scattering

In this section we present a Euclidean approach to high-energy reactions of color-dipoles in the eikonal approximation. After a short review of the functional integral approach to high-energy dipole-dipole scattering in Minkowski space-time, we generalize the analytic continuation introduced by Meggiolaro [24] from parton-parton scattering to dipole-dipole scattering. This shows how one can access high-energy reactions directly in lattice QCD. We apply this approach to compute the scattering of dipoles in the fundamental and adjoint representation of $SU(N_c)$ at high-energy in the Euclidean LLCM. The result shows the consistency with the analytic continuation of the gluon field strength correlator used in all earlier applications of the SVM and LLCM to high-energy scattering. Finally, we comment on the QCD van der Waals potential which appears in the limiting case of two static color-dipoles.

In *Minkowski space-time*, high-energy reactions of color-dipoles in the eikonal approximation have been considered — as basis for hadron-hadron, photon-hadron, and photon-photon reactions — in the functional integral approach to high-energy collisions developed originally for parton-parton scattering [5, 6] and then extended to gauge-invariant dipole-dipole scattering [7–9]. The corresponding T -matrix element for the elastic scattering of two color-dipoles at transverse momentum transfer \vec{q}_\perp ($t = -\vec{q}_\perp^2$) and c.m. energy squared s reads

$$T_{r_1 r_2}^M(s, t, z_1, \vec{r}_{1\perp}, z_2, \vec{r}_{2\perp}) = 2is \int d^2 b_\perp e^{i\vec{q}_\perp \cdot \vec{b}_\perp} \left[1 - S_{r_1 r_2}^M(s, \vec{b}_\perp, z_1, \vec{r}_{1\perp}, z_2, \vec{r}_{2\perp}) \right] \quad (5.1)$$

with the S -matrix element (M refers to Minkowski space-time)

$$S_{r_1 r_2}^M(s, \vec{b}_\perp, z_1, \vec{r}_{1\perp}, z_2, \vec{r}_{2\perp}) = \lim_{T \rightarrow \infty} \frac{\langle W_{r_1}[C_1] W_{r_2}[C_2] \rangle_M}{\langle W_{r_1}[C_1] \rangle_M \langle W_{r_2}[C_2] \rangle_M} . \quad (5.2)$$

The color-dipoles are considered in the $SU(N_c)$ representation r_i and have transverse size and orientation $\vec{r}_{i\perp}$. The longitudinal momentum fraction carried by the quark

of dipole i is z_i . (Here and in the following we use several times the term quark generically for color-sources in an arbitrary $SU(N_c)$ representation.) The impact parameter between the dipoles is [30]

$$\vec{b}_\perp = \vec{r}_{1q} + (1 - z_1)\vec{r}_{1\perp} - \vec{r}_{2q} - (1 - z_2)\vec{r}_{2\perp} = \vec{r}_{1cm} - \vec{r}_{2cm} , \quad (5.3)$$

where \vec{r}_{iq} ($\vec{r}_{i\bar{q}}$) is the transverse position of the quark (antiquark), $\vec{r}_{i\perp} = \vec{r}_{i\bar{q}} - \vec{r}_{iq}$, and $\vec{r}_{icm} = z_i\vec{r}_{iq} + (1 - z_i)\vec{r}_{i\bar{q}}$ is the center of light-cone momenta. Figure 6 illustrates the (a) space-time and (b) transverse arrangement of the dipoles. The dipole trajectories C_i are described as straight lines. This is a good approximation as long as the kinematical assumption behind the eikonal approximation, $s \gg -t$, holds that allows us to neglect the change of the dipole velocities $v_i = p_i/m$ in the scattering process, where p_i is the momentum and m the mass of the considered dipole. Moreover, the paths C_i are considered light-like⁸ in line with the high-energy limit, $m^2 \ll s \rightarrow \infty$. For the *hyperbolic angle* or *rapidity gap* between the dipole trajectories $\gamma = (\vec{v}_1 \cdot \vec{v}_2)$ — which is the central quantity in the analytic continuation discussed below and also defined through $s = 4m^2 \cosh^2(\gamma/2)$ — the high-energy limit implies

$$\lim_{m^2 \ll s \rightarrow \infty} \gamma \approx \ln(s/m^2) \rightarrow \infty . \quad (5.4)$$

The QCD VEV's $\langle \dots \rangle_M$ in the S -matrix element (5.2) represent *Minkowskian* functional integrals [6] in which — as in the Euclidean case discussed above — the functional integration over the fermion fields has already been carried out.

The Euclidean approach to the described elastic scattering of dipoles in the eikonal approximation is based on *Meggiolaro's analytic continuation* of the high-energy parton-parton scattering amplitude [24]. Meggiolaro's analytic continuation has been derived in the functional integral approach to high-energy collisions [5, 6] in which parton-parton scattering is described in terms of Wegner-Wilson lines: The Minkowskian amplitude, $g^M(\gamma, T, t)$, given by the expectation value of two Wegner-Wilson lines, forming an hyperbolic angle γ in Minkowski space-time, and the Euclidean “amplitude,” $g^E(\Theta, T, t)$, given by the expectation value of two Wegner-Wilson lines, forming an angle $\Theta \in [0, \pi]$ in Euclidean space-time, are connected by the following analytic continuation in the angular variables and the temporal extension T , which is needed as an IR regulator in the case of Wegner-Wilson lines,

$$g^E(\Theta, T, t) = g^M(\gamma \rightarrow i\Theta, T \rightarrow -iT, t) , \quad (5.5)$$

$$g^M(\gamma, T, t) = g^E(\Theta \rightarrow -i\gamma, T \rightarrow iT, t) . \quad (5.6)$$

⁸In fact, exactly light-like trajectories ($\gamma \rightarrow \infty$) are considered in most applications of the functional integral approach to high-energy collisions [4, 7–9, 22, 23, 29–33]. A detailed investigation of the more general case of finite rapidity γ can be found in [33].

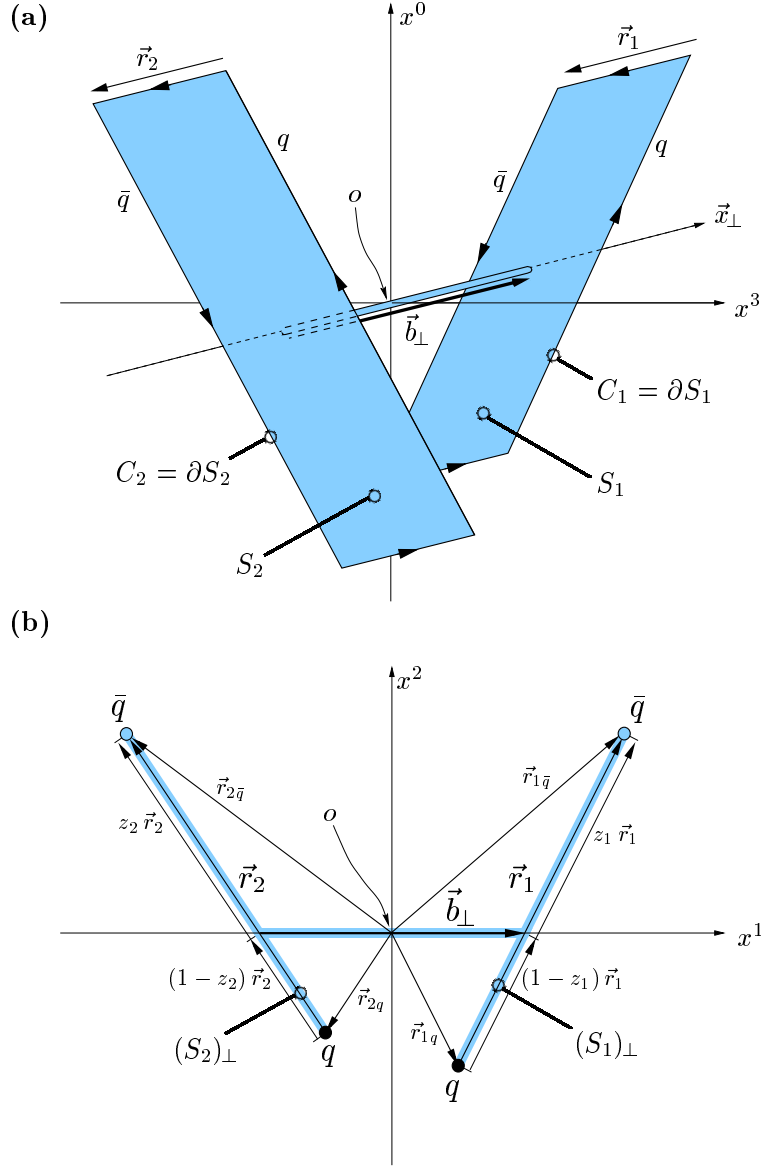


Figure 6: High-energy dipole-dipole scattering in the eikonal approximation represented by Wegner-Wilson loops in the fundamental representation of $SU(N_c)$: (a) space-time and (b) transverse arrangement of the Wegner-Wilson loops. The shaded areas represent the strings extending from the quark to the antiquark path in each color dipole. The thin tube allows us to compare the field strengths in surface S_1 with the field strengths in surface S_2 . The impact parameter \vec{b}_\perp connects the centers of light-cone momenta of the dipoles.

Generalizing this relation to *gauge-invariant* dipole-dipole scattering described in terms of Wegner-Wilson loops, the IR divergence known from the case of Wegner-Wilson lines vanishes and no finite IR regulator T is necessary. Thus, the Minkowskian S -matrix element (5.2), given by the expectation values of two Wegner-Wilson loops, forming an hyperbolic angle γ in Minkowski space-time, can be computed from the Euclidean “ S -matrix element”

$$S_{r_1 r_2}^E(\Theta, \vec{b}_\perp, z_1, \vec{r}_{1\perp}, z_2, \vec{r}_{2\perp}) = \lim_{T \rightarrow \infty} \frac{\langle W_{r_1}[C_1] W_{r_2}[C_2] \rangle_E}{\langle W_{r_1}[C_1] \rangle_E \langle W_{r_2}[C_2] \rangle_E} \quad (5.7)$$

given by the expectation values of two Wegner-Wilson loops, forming an angle $\Theta \in [0, \pi]$ in Euclidean space-time, via an analytic continuation in the angular variable

$$S_{r_1 r_2}^M(\gamma \approx \ln[s/m^2], \vec{b}_\perp, z_1, \vec{r}_{1\perp}, z_2, \vec{r}_{2\perp}) = S_{r_1 r_2}^E(\Theta \rightarrow -i\gamma, \vec{b}_\perp, z_1, \vec{r}_{1\perp}, z_2, \vec{r}_{2\perp}) , \quad (5.8)$$

where E indicates Euclidean space-time and the QCD VEV's $\langle \dots \rangle_E$ represent Euclidean functional integrals that are equivalent to the ones denoted by $\langle \dots \rangle_G$ in the preceding sections, i.e., in which the functional integration over the fermion fields has already been carried out.

The angle Θ is best illustrated in the relation of the Euclidean S -matrix element (5.7) to the van der Waals potential between two static dipoles, $V_{r_1 r_2}(\Theta = 0, \vec{b}, z_1, \vec{r}_1, z_2, \vec{r}_2)$, discussed at the end of this section,

$$S_{r_1 r_2}^E(\Theta, \vec{b}_\perp, z_1, \vec{r}_{1\perp}, z_2, \vec{r}_{2\perp}) = \lim_{T \rightarrow \infty} \exp \left[-T V_{r_1 r_2}(\Theta, \vec{b}_\perp, z_1, \vec{r}_{1\perp}, z_2, \vec{r}_{2\perp}) \right] . \quad (5.9)$$

Figure 7 shows the loop-loop geometry necessary to compute $S_{r_1 r_2}^E(\Theta \neq 0, \dots)$ and how it is obtained by generalizing the geometry relevant for the computation of the potential between two static dipoles ($\Theta = 0$): While the potential between two static dipoles is computed from two loops along parallel “temporal” unit vectors, $t_1 = t_2 = (0, 0, 0, 1)$, the Euclidean S -matrix element (5.7) involves the tilting of one of the two loops, e.g., the tilting of t_1 by the angle Θ towards the X_3 -axis, $t_1 = (0, 0, -\sin \Theta, \cos \Theta)$. The “temporal” unit vectors t_i are also discussed in Appendix B together with another illustration of the tilting angle Θ .

Since the Euclidean S -matrix element (5.7) involves only configurations of Wegner-Wilson loops in Euclidean space-time and *Euclidean* functional integrals, it can be computed directly on a Euclidean lattice. First attempts in this direction have been carried out but only very few signals could be extracted, while most of the data was dominated by noise [28]. Once precise results are available, the analytic continuation (5.8) will allow us to access hadronic high-energy reactions directly in lattice QCD, i.e., within a non-perturbative description of QCD from first principles. More generally, the presented gauge-invariant analytic continuation (5.8)

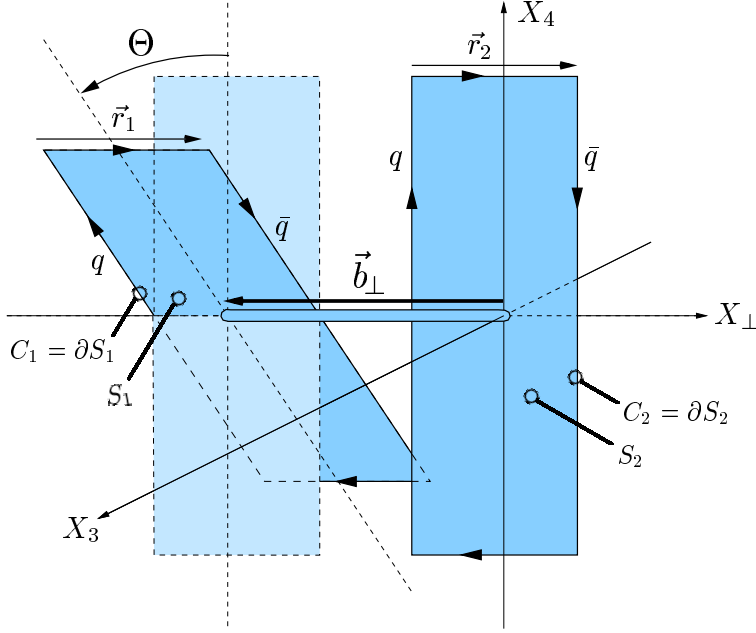


Figure 7: The loop-loop geometry necessary to compute $S_{r_1 r_2}^E(\Theta \neq 0, \dots)$ illustrated as a generalization of the geometry relevant for the computation of the van der Waals potential between two static dipoles ($\Theta = 0$). While the potential between two static dipoles is computed from two loops along parallel “temporal” unit vectors, $t_1 = t_2 = (0, 0, 0, 1)$, the Euclidean S -matrix element (5.7) involves the tilting of one of the two loops, e.g., the tilting of t_1 by the angle Θ towards the X_3 -axis, $t_1 = (0, 0, -\sin \Theta, \cos \Theta)$.

makes any approach limited to a Euclidean formulation of the theory applicable for investigations of high-energy reactions. Indeed, Meggioraro’s analytic continuation has already been used to access high-energy scattering from the supergravity side of the AdS/CFT correspondence [25], which requires a positive definite metric in the definition of the minimal surface [26], and to examine the effect of instantons on high-energy scattering [27].

Let us now perform the analytic continuation explicitly in our Euclidean model. For the scattering of two color-dipoles in the *fundamental representation* of $SU(N_c)$, the Euclidean S -matrix element becomes with the VEV’s (2.14) and (2.35)

$$\begin{aligned}
S_{DD}^E(\Theta, \vec{b}_\perp, z_1, \vec{r}_{1\perp}, z_2, \vec{r}_{2\perp}) &:= S_{N_c N_c}^E(\Theta, \vec{b}_\perp, z_1, \vec{r}_{1\perp}, z_2, \vec{r}_{2\perp}) \\
&= \lim_{T \rightarrow \infty} \left(\frac{N_c + 1}{2N_c} \exp \left[-\frac{N_c - 1}{2N_c} \chi_{S_1 S_2} \right] + \frac{N_c - 1}{2N_c} \exp \left[\frac{N_c + 1}{2N_c} \chi_{S_1 S_2} \right] \right) \quad (5.10)
\end{aligned}$$

where $\chi_{S_i S_j}$ — defined in (2.27) — decomposes into a perturbative (P) and non-perturbative (NP) component according to our decomposition of the gluon field

strength correlator (2.42),

$$\chi_{S_1 S_2} = \chi_{S_1 S_1}^P + \chi_{S_1 S_2}^{NP} = \chi_{S_1 S_2}^P + (\chi_{S_1 S_2}^{NP\ nc} + \chi_{S_1 S_2}^{NP\ c}) . \quad (5.11)$$

In the limit $T_1 = T_2 = T \rightarrow \infty$ and for $\Theta \in [0, \pi]$, the components read

$$\chi_{S_1 S_2}^P = \cot \Theta \chi^P , \quad \chi_{S_1 S_2}^{NP\ nc} = \cot \Theta \chi^{NP\ nc} , \quad \chi_{S_i S_j}^{NP\ c} = \cot \Theta \chi^{NP\ c} \quad (5.12)$$

with

$$\begin{aligned} \chi^P = & \left[g^2 D_P'^{(2)}(|\vec{r}_{1q} - \vec{r}_{2\bar{q}}|) + g^2 D_P'^{(2)}(|\vec{r}_{1\bar{q}} - \vec{r}_{2q}|) \right. \\ & \left. - g^2 D_P'^{(2)}(|\vec{r}_{1q} - \vec{r}_{2q}|) - g^2 D_P'^{(2)}(|\vec{r}_{1\bar{q}} - \vec{r}_{2\bar{q}}|) \right] \end{aligned} \quad (5.13)$$

$$\begin{aligned} \chi^{NP\ nc} = & \frac{\pi^2 G_2(1 - \kappa)}{3(N_c^2 - 1)} \left[D_1'^{(2)}(|\vec{r}_{1q} - \vec{r}_{2\bar{q}}|) + D_1'^{(2)}(|\vec{r}_{1\bar{q}} - \vec{r}_{2q}|) \right. \\ & \left. - D_1'^{(2)}(|\vec{r}_{1q} - \vec{r}_{2q}|) - D_1'^{(2)}(|\vec{r}_{1\bar{q}} - \vec{r}_{2\bar{q}}|) \right] \end{aligned} \quad (5.14)$$

$$\chi^{NP\ c} = \frac{\pi^2 G_2 \kappa}{3(N_c^2 - 1)} (\vec{r}_1 \cdot \vec{r}_2) \int_0^1 dv_1 \int_0^1 dv_2 D^{(2)}(|\vec{r}_{1q} + v_1 \vec{r}_{1\perp} - \vec{r}_{2q} - v_2 \vec{r}_{2\perp}|) \quad (5.15)$$

as derived explicitly in Appendix C with the minimal surfaces illustrated in Fig. 7. In Eq. (5.13) the shorthand notation $g^2 D_P'^{(2)}(|\vec{Z}_\perp|) = g^2(|\vec{Z}_\perp|) D_P'^{(2)}(|\vec{Z}_\perp|)$ is used with $g^2(|\vec{Z}_\perp|)$ again understood as the running coupling (2.47). The transverse Euclidean correlation functions

$$D_x^{(2)}(\vec{Z}^2) := \int \frac{d^4 K}{(2\pi)^2} e^{iKZ} \tilde{D}_x(K^2) \delta(K_3) \delta(K_4) \quad (5.16)$$

are obtained from the (massive) gluon propagator (2.43) and the exponential correlation function (2.50)

$$D_P'^{(2)}(\vec{Z}_\perp^2) = \frac{1}{2\pi} K_0(m_G |\vec{Z}_\perp|) \quad (5.17)$$

$$D_1'^{(2)}(\vec{Z}_\perp^2) = \pi a^4 \left(3 + 3 \frac{|\vec{Z}_\perp|}{a} + \frac{|\vec{Z}_\perp|^2}{a^2} \right) \exp\left(-\frac{|\vec{Z}_\perp|}{a}\right) \quad (5.18)$$

$$D^{(2)}(\vec{Z}_\perp^2) = 2\pi a^2 \left(1 + \frac{|\vec{Z}_\perp|}{a} \right) \exp\left(-\frac{|\vec{Z}_\perp|}{a}\right) \quad (5.19)$$

With the full Θ -dependence exposed in (5.12), the analytic continuation (5.8) reads

$$\chi_{S_1 S_2} = \cot \Theta \chi \xrightarrow{\Theta \rightarrow -i\gamma} \cot(-i\gamma) \chi \xrightarrow{s \rightarrow \infty} i\chi \quad (5.20)$$

and leads to the desired Minkowskian S -matrix element for elastic dipole-dipole scattering (DD) in the high-energy limit in which the dipoles move on the light-cone

$$\begin{aligned}
\lim_{s \rightarrow \infty} S_{DD}^M(s, \vec{b}_\perp, z_1, \vec{r}_{1\perp}, z_2, \vec{r}_{2\perp}) &:= \lim_{s \rightarrow \infty} S_{N_c N_c}^M(s, \vec{b}_\perp, z_1, \vec{r}_{1\perp}, z_2, \vec{r}_{2\perp}) \\
&= S_{DD}^E(\cot \Theta \rightarrow i, \vec{b}_\perp, z_1, \vec{r}_{1\perp}, z_2, \vec{r}_{2\perp}) \\
&= \lim_{T \rightarrow \infty} \left(\frac{N_c + 1}{2N_c} \exp \left[-i \frac{N_c - 1}{2N_c} \chi \right] + \frac{N_c - 1}{2N_c} \exp \left[i \frac{N_c + 1}{2N_c} \chi \right] \right) \quad (5.21)
\end{aligned}$$

where $\chi = \chi^P + \chi^{NP \text{ nc}} + \chi^{NP \text{ c}}$ with (5.13), (5.14), and (5.15).

It is striking that exactly the same result has been obtained in [4]⁹ with the alternative analytic continuation introduced for applications of the SVM to high-energy reactions [7–9]. In this complementary approach the gauge-invariant bilocal gluon field strength correlator is analytically continued from Euclidean to Minkowskian space-time by the substitution $\delta_{\mu\rho} \rightarrow -g_{\mu\rho}$ and the analytic continuation of the Euclidean correlation functions to real time $D_x^E(Z^2) \rightarrow D_x^M(z^2)$. In the subsequent steps, one finds $\langle W[C] \rangle_M = 1$ due to the light-likeness of the loops and that the longitudinal correlations can be integrated out $\langle W_{r_1}[C_1] W_{r_2}[C_2] \rangle_M = f(s, \vec{b}_\perp, \dots)$. One is left with exactly the Euclidean correlations in transverse space that have been obtained above. This confirms the analytic continuation used in the earlier LLCM investigations in Minkowski space-time [4, 22, 23] and in all earlier SVM applications to high-energy scattering [7–9, 29–34].

In the limit of small χ -functions, $|\chi^P| \ll 1$ and $|\chi^{NP}| \ll 1$, (5.21) reduces to

$$\lim_{s \rightarrow \infty} S_{DD}^M(s, \vec{b}_\perp, z_1, \vec{r}_{1\perp}, z_2, \vec{r}_{2\perp}) \approx 1 + \frac{N_c^2 - 1}{8N_c^2} \chi^2 = 1 + \frac{C_2(N_c)}{4N_c} \chi^2. \quad (5.22)$$

The perturbative correlations, $(\chi^P)^2$, describe the well-known *two-gluon exchange* contribution [68, 69] to dipole-dipole scattering, which is, of course, an important successful cross-check of the presented Euclidean approach to high-energy scattering. The non-perturbative correlations, $(\chi^{NP})^2$, describe the corresponding non-perturbative two-point interactions that contain contributions of the confining QCD string to dipole-dipole scattering. We have analysed these string contributions systematically as manifestations of confinement in high-energy scattering reactions in our previous work [23].

⁹To see this identity, recall that $\langle W[C] \rangle = 1$ for light-like loops and consider in [4] the result (2.30) for the loop-loop correlation function (2.3) together with the χ -function (2.40) and its components given in (2.49), (2.54), and (2.57) with the transverse Minkowskian correlation functions (2.50), (2.55), and (2.58).

From the small- χ limit, one sees that the full S -matrix element (5.21) describes multiple gluonic interactions. Indeed, the higher order terms in the expansion of the exponential functions ensure the fundamental S -matrix unitarity condition in impact parameter space as shown discussed in [4, 31].

Concerning the energy dependence, the S -matrix element (5.21) leads to energy-independent cross sections in contradiction to the experimental observation. Although disappointing from the phenomenological point of view, this is not surprising since our approach does not describe explicit gluon radiation needed for a non-trivial energy dependence. However, based on the S -matrix element (5.21), a phenomenological energy dependence can be constructed that allows a unified description of high-energy hadron-hadron, photon-hadron, and photon-photon reactions and an investigation of saturation effects in hadronic cross sections manifesting the S -matrix unitarity [4, 22]. This, of course, can only be an intermediate step. For a more fundamental understanding of hadronic high-energy reactions in our model, gluon radiation and quantum evolution have to be implemented explicitly.

Although the scattering of two color-dipoles in the fundamental representation of $SU(N_c)$ is, of course, the most relevant case, we can derive immediately also the Minkowskian S -matrix element for the scattering of a fundamental (D) and an adjoint dipole (“glueball” GB) in the Euclidean LLCM. Using (2.40) and proceeding otherwise as above, we find in the high-energy limit

$$\begin{aligned} \lim_{s \rightarrow \infty} S_{DGB}^M(s, \vec{b}, z_1, \vec{r}_1, z_2, \vec{r}_2) &:= \lim_{s \rightarrow \infty} S_{N_c N_c - 1}^M(\Theta, \vec{b}, z_1, \vec{r}_1, z_2, \vec{r}_2) \\ &= \lim_{T \rightarrow \infty} \left(\frac{1}{N_c^2 - 1} \exp\left[i \frac{N_c}{2} \chi\right] + \frac{N_c + 2}{2(N_c + 1)} \exp\left[-i \frac{1}{2} \chi\right] + \frac{N_c - 2}{2(N_c - 1)} \exp\left[i \frac{1}{2} \chi\right] \right). \end{aligned} \quad (5.23)$$

where $\chi = \chi^P + \chi^{NPnc} + \chi^{NPc}$ with (5.13), (5.14), and (5.15).

Finally, we would like to comment on the *van der Waals interaction* of two color-dipoles, which is — as already mentioned — related to the Euclidean S -matrix element in the limiting case of $\Theta = 0$ as can be seen from (5.9): The QCD van der Waals potential between two static dipoles can be expressed in terms of Wegner-Wilson loops [70, 71]

$$V_{r_1 r_2}(\Theta = 0, \vec{b}, z_1 = 1/2, \vec{r}_1, z_2 = 1/2, \vec{r}_2) = - \lim_{T \rightarrow \infty} \frac{1}{T} \ln \frac{\langle W_{r_1}[C_1] W_{r_2}[C_2] \rangle}{\langle W_{r_1}[C_1] \rangle \langle W_{r_2}[C_2] \rangle}. \quad (5.24)$$

In this limit ($\Theta = 0$) intermediate octet states and their limited lifetime become important as is well known from perturbative computations of the QCD van der Waals potential between two static color-dipoles [70–72]: Working with static dipoles, i.e., infinitely heavy color-sources, there is an energy degeneracy between the intermediate octet states and the initial (final) singlet states that leads for perturbative

two-gluon exchange to a linear divergence in T as $T \rightarrow \infty$. This IR divergence can be lifted by introducing manually an energy gap between the singlet ground state and the excited octet state and thus a limit on the lifetime of the intermediate octet state [70–72].

In the perturbative limit of $g^2 \rightarrow 0$ and T large but finite, i.e., $\chi^P \ll 1$, the perturbative component of our model describes the two-gluon exchange contribution to the van der Waals potential which is plagued by this IR divergence due to the static limit. In the more general case of g^2 finite and $T \rightarrow \infty$, which is applicable also for the non-perturbative component of our model, one cannot use the small- χ limit and multiple gluonic interactions become important. Here, our perturbative component describes multiple gluon exchanges that reduce to an effective one-gluon exchange contribution to the van der Waals potential whose interaction range ($\propto 1/m_G$) contradicts the common expectations. Indeed, it is also in contradiction to our results for the glueball mass M_{GB} which determines the interaction range ($\propto 1/M_{GB}$) between two color-dipoles for large dipole separations. As already mentioned in Sec. 2.3, we find for the perturbative component, $M_{GB}^P = 2m_G$, i.e., half of the interaction range of one-gluon exchange, by computing the exponential decay of the correlation of two small quadratic loops $P_{r_i}^{\alpha\beta}$ for large Euclidean times $\tau \rightarrow \infty$

$$M_{GB} := - \lim_{\tau \rightarrow \infty} \frac{1}{\tau} \ln \frac{\langle P_{r_1}^{\alpha\beta}(0) P_{r_2}^{\alpha\beta}(\tau) \rangle}{\langle P_{r_1}^{\alpha\beta}(0) \rangle \langle P_{r_2}^{\alpha\beta}(\tau) \rangle} . \quad (5.25)$$

Note that we find for the non-perturbative component, $M_{GB}^{NP} = 2/a$, which is smaller than $M_{GB}^P = 2m_G$ with the LLCM parameters and thus governs the long range correlations in the LLCM.

Thus, for a meaningful investigation of the QCD van der Waals forces within our model, one has to go beyond the static limit in order to describe the limited lifetime of the intermediate octet states appropriately. This we postpone for future work since the focus in this work is on high-energy scattering where the gluons are always exchanged within a short time interval due to the light-likeness of the scattered particles and the finite correlations lengths. Nevertheless, going beyond the static limit in the dipole-dipole potential means going beyond the eikonal approximation in high-energy scattering and it is, of course, of utmost importance to see how such generalizations alter our results.

6 Conclusion

We have introduced the Euclidean version of the loop-loop correlation model (LLCM) [4] in which the QCD vacuum is described by perturbative gluon exchange and the

non-perturbative stochastic vacuum model (SVM) [12]. This combination leads to a static quark-antiquark potential with color-Coulomb behavior for small and confining linear rise for large source separations in good agreement with lattice QCD results. We have computed in the LLCM the vacuum expectation value of one Wegner-Wilson loop, $\langle W_r[C] \rangle$, and the correlation of two Wegner-Wilson loops, $\langle W_{r_1}[C_1] W_{r_2}[C_2] \rangle$, for arbitrary loop geometries and general representations $r_{(i)}$ of $SU(N_c)$. Specifying the loop geometries, these results allow us to compute the static quark-antiquark potential, the glueball mass, the chromo-field distributions of static color-dipoles, the QCD van der Waals potential between two static color-dipoles, and the S -matrix element for high-energy dipole-dipole scattering.

We have applied the LLCM to compute the chromo-electric fields generated by a static color-dipole in the fundamental and adjoint representation of $SU(N_c)$. The formation of a confining color-flux tube is described by the non-perturbative SVM correlations [15] and the color-Coulomb field is obtained from perturbative gluon exchange. We have found Casimir scaling for both the perturbative and non-perturbative contributions to the chromo-electric fields in agreement with recent lattice data [55]. String breaking is neither described for sources in the fundamental representation nor for sources in the adjoint representation which indicates that in our approach not only dynamical fermions (quenched approximation) are missing but also some gluon dynamics. Transverse and longitudinal energy density profiles have been provided: For small dipoles, $R = 0.1$ fm, perturbative physics dominates and non-perturbative correlations are negligible. For large dipoles, $R \gtrsim 1$ fm, the non-perturbative confining string dominates the chromo-electric fields between the color-sources. The transition from perturbative to string behavior takes place at source separations of about 0.5 fm in agreement with the recent results of Lüscher and Weisz [16]. The root mean squared radius R_{ms} of the confining string and the energy density in the center of a fundamental $SU(3)$ dipole $\varepsilon_3(X=0)$ are governed completely by non-perturbative physics for large R and saturate as R increases at $R_{ms}^{R \rightarrow \infty} \approx 0.55$ fm and $\varepsilon_3^{R \rightarrow \infty}(X=0) \approx 1$ GeV/fm³.

We have presented the low-energy theorems [18–20], known in lattice QCD as Michael sum rules [17], in their complete form in continuum theory taking into account the important contributions found in [18, 21] that are missing in the original formulation [17]. We have used the complete theorems to compare the energy and action stored in the confining string with the confining part of the static quark-antiquark potential. The comparison shows consistency of the model results and indicates that the non-perturbative SVM component is working at the renormalization scale at which $\beta(g)/g = -2$ and $\alpha_s = 0.81$. Earlier SVM investigations along these lines have found a different value of $\alpha_s = 0.57$ with the pyramid mantle choice for the surface [15, 21] but were incomplete since only the contribution from the

traceless part of the energy-momentum tensor has been considered in the energy sum.

An Euclidean approach to high-energy dipole-dipole scattering has been established by generalizing Meggiolaro’s analytic continuation [24] from parton-parton scattering to gauge-invariant dipole-dipole scattering. The generalized analytic continuation allows us to derive S -matrix elements for high-energy reactions from configurations of Wegner-Wilson loops in Euclidean space-time with Euclidean functional integrals. It thus shows how one can access high-energy reactions directly in lattice QCD. First attempts in this direction have already been carried out but only very few signals could be extracted, while most of the data was dominated by noise [28]. We have applied this approach to compute in the Euclidean LLCM the scattering of dipoles at high-energy. The result derived in the Minkowskian version of the LLCM [4] has been exactly recovered including the well-known two-gluon exchange contribution to dipole-dipole scattering [68, 69]. This confirms the analytic continuation of the gluon field strength correlator used in all earlier applications of the SVM to high-energy scattering [7–9, 29–34].

The S -matrix element obtained in our approach has already been used to investigate manifestations of the confining QCD string in high-energy reactions of photons and hadrons [23] but leads to energy-independent cross sections in contradiction to the experimental observation [4]. The missing energy dependence is disappointing but not surprising since our approach does not describe explicit gluon radiation needed for a non-trivial energy dependence. In our previous work we have introduced a phenomenological energy dependence into the S -matrix element that allows a unified description of hadron-hadron, photon-hadron, and photon-photon reactions and respects the S -matrix unitarity condition in impact parameter space [4, 22]. However, for a more fundamental understanding of hadronic high-energy reactions in our model, one faces the highly ambitious task to implement gluon radiation and quantum evolution explicitly.

More generally, the presented Euclidean approach to high-energy scattering makes any method limited to a Euclidean formulation of the theory applicable for investigations of high-energy reactions. Here encouraging new results have been obtained with instantons [27] and within the AdS/CFT correspondence [25] and it will be interesting to see precise results from the lattice. A promising complementary Euclidean approach has been proposed in [73] where the structure functions of deep inelastic scattering at small Bjorken x are related to an effective Euclidean field theory. Here one hopes that the limit $x \rightarrow 0$ corresponds to critical behavior in the effective theory. The aim is again to provide a framework in which structure functions can be calculated from first principles using genuine non-perturbative methods such as lattice computations. In another recent attempt, the energy dependence of

the proton structure function has been related successfully to critical properties of an effective near light-cone Hamiltonian in a non-perturbative lattice approach [74]. It will be interesting to see further developments along these lines aiming at an understanding of hadronic high-energy scattering from the QCD Lagrangian.

Acknowledgements

We would like to thank N. Brambilla, A. Di Giacomo, C. Ewerz, H. Forkel, M. Jamin, E. Meggiolaro, O. Nachtmann, Yu. Simonov, I. Stamatescu, and A. Vairo for stimulating discussions and G. Bali for helpful comments and providing us with lattice data. We thank F. Schwab for the careful reading of the manuscript. This research is partially funded by the INTAS project “Non-Perturbative QCD” and the European TMR Contract HPRN-CT-2000-00130.

A The Static Color-Dipole Potential

In this Appendix the QCD potential of static color-dipoles in the fundamental and adjoint representation of $SU(N_c)$ is computed in our model. Color-Coulomb behavior is found for small dipole sizes and the confining linear rise for large dipole sizes. Casimir scaling is obtained in agreement with lattice QCD investigations.

As already explained in Sec. 3, the static color-dipole — two static color-sources separated by a distance R in a net color-singlet state — is described by a Wegner-Wilson loop $W_r[C]$ with a rectangular path C of spatial extension R and temporal extension $T \rightarrow \infty$ where r indicates the $SU(N_c)$ representation of the considered sources. Figure 8 illustrates a static color-dipole in the fundamental representation $r = N_c$. The potential of the static color-dipole is obtained from the VEV of the corresponding Wegner-Wilson loop [11, 66]

$$V_r(R) = - \lim_{T \rightarrow \infty} \frac{1}{T} \ln \langle W_r[C] \rangle_{\text{pot}} , \quad (\text{A.1})$$

where “pot” indicates the subtraction of the self-energy of the color-sources. The static quark-antiquark potential $V_r = V_{N_c}$ is obtained from a loop in the fundamental representation and the potential of a static gluino pair $V_r = V_{N_c^2-1}$ from a loop in the adjoint representation.

With our result for $\langle W_r[C] \rangle$, (2.14), obtained with the Gaussian approximation

in the gluon field strength, the static potential reads

$$V_r(R) = \frac{C_2(r)}{2} \lim_{T \rightarrow \infty} \frac{1}{T} \chi_{SS\text{pot}} , \quad (\text{A.2})$$

with the self-energy subtracted, i.e, $\chi_{SS\text{pot}} := \chi_{SS} - \chi_{SS\text{self}}$ (see Appendix C). According to the structure of the gluon field strength correlator, (2.12) and (2.42), there are perturbative (P) and non-perturbative (NP) contributions to the static potential

$$V_r(R) = \frac{C_2(r)}{2} \lim_{T \rightarrow \infty} \frac{1}{T} \{ \chi_{SS\text{pot}}^P + (\chi_{SS\text{pot}}^{NP\text{ } nc} + \chi_{SS\text{pot}}^{NP\text{ } c}) \} , \quad (\text{A.3})$$

where the explicit form of the χ -functions is given in Eqs. (C.9), (C.28), and (C.37).

The perturbative contribution to the static potential describes the *color-Yukawa potential* (which reduces to the *color-Coulomb potential* for $m_G = 0$)

$$V_r^P(R) = -C_2(r) \frac{g^2(R)}{4\pi R} \exp[-m_G R] . \quad (\text{A.4})$$

Here we have used the result for $\chi_{SS\text{pot}}^P$ given in (C.37) and the perturbative correlation function

$$D_P'^{(3)}(\vec{Z}^2) := \int \frac{d^4 K}{(2\pi)^3} e^{iKZ} \tilde{D}_P'^{(3)}(K^2) \delta(K_4) = - \frac{\exp[-m_G |\vec{Z}|]}{4\pi |\vec{Z}|} \quad (\text{A.5})$$

which is obtained from the massive gluon propagator (2.43). As shown below, the perturbative contribution dominates the static potential for small dipoles sizes R .

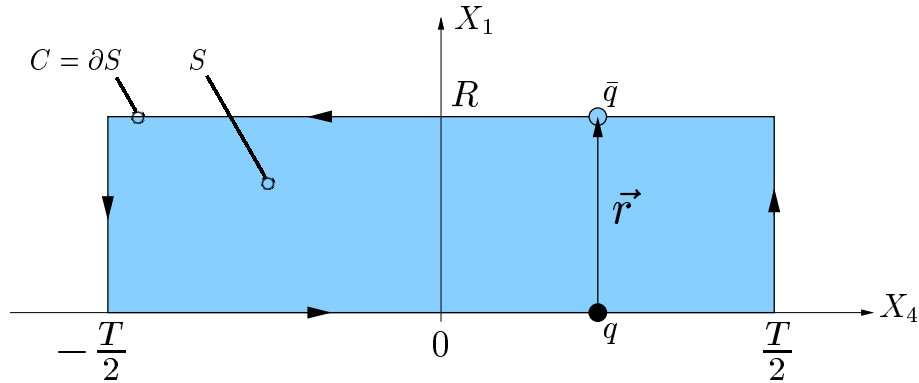


Figure 8: A static color-dipole of size R in the fundamental representation. The rectangular path C of spatial extension R and temporal extension T indicates the world-line of the dipole described the Wegner-Wilson loop $W_{N_c}[C]$. The shaded area bounded by the loop $C = \partial S$ represents the minimal surface S used to compute the static dipole potential.

The non-perturbative contributions to the static potential, the *non-confining* component (*nc*) and the *confining* component (*c*), read

$$V_r^{NP\ nc}(R) = C_2(r) \frac{\pi^2 G_2 (1 - \kappa)}{3(N_c^2 - 1)} D_1'^{(3)}(R^2) \quad (\text{A.6})$$

$$V_r^{NP\ c}(R) = C_2(r) \frac{\pi^2 G_2 \kappa}{3(N_c^2 - 1)} \int_0^R d\rho (R - \rho) D^{(3)}(\rho^2), \quad (\text{A.7})$$

where we have used the results for $\chi_{SS_{\text{pot}}}^{NP\ nc}$ and $\chi_{SS_{\text{pot}}}^{NP\ c} = \chi_{SS}^{NP\ c}$ given respectively in (C.28) and (C.9) obtained with the minimal surface, i.e., the planar surface bounded by the loop as indicated by the shaded area in Fig. 8. With the exponential correlation function (2.50), the correlation function in (A.6) reads

$$D_1'^{(3)}(\vec{Z}^2) := \int \frac{d^4 K}{(2\pi)^3} e^{iKZ} \tilde{D}_1'^{(3)}(K^2) \delta(K_4) = -a |\vec{Z}|^2 K_2[|\vec{Z}|/a], \quad (\text{A.8})$$

and the correlation function in (A.7) is given in (3.19). For large dipole sizes, $R \gtrsim 0.5$ fm, the non-confining contribution (A.6) vanishes exponentially while the confining contribution (A.7) — as anticipated — leads to *confinement* [12], i.e., the confining linear increase,

$$V_r^{NP\ c}(R) \Big|_{R \gtrsim 0.5 \text{ fm}} = \sigma_r R + \text{const.} \quad (\text{A.9})$$

Thus, the QCD *string tension* is given by the confining SVM component [12] and reads for a color-dipole in the representation r of $SU(N_c)$

$$\sigma_r = C_2(r) \frac{\pi^3 G_2 \kappa}{48} \int_0^\infty dZ^2 D(Z^2) = C_2(r) \frac{\pi^3 \kappa G_2 a^2}{24}, \quad (\text{A.10})$$

where the exponential correlation function (2.50) is used in the final step. Since the string tension can be computed from first principles within lattice QCD [50], relation (A.10) puts an important constraint on the three fundamental parameters of the non-perturbative QCD vacuum a , G_2 , and κ . With the values for a , G_2 , and κ given in (2.51), that are used throughout this work, one obtains for the string tension of the $SU(3)$ quark-antiquark potential ($r = 3$) a reasonable value of

$$\sigma_3 = 0.22 \text{ GeV}^2 \equiv 1.12 \text{ GeV/fm} \quad (\text{A.11})$$

The static $SU(N_c = 3)$ quark-antiquark potential $V_{N_c}(R) = V_3(R)$ is shown as a function of the quark-antiquark separation R in Fig. 9, where the solid, dotted, and dashed lines indicate the full static potential and its perturbative and non-perturbative contributions, respectively. For small quark-antiquark separations $R \lesssim$

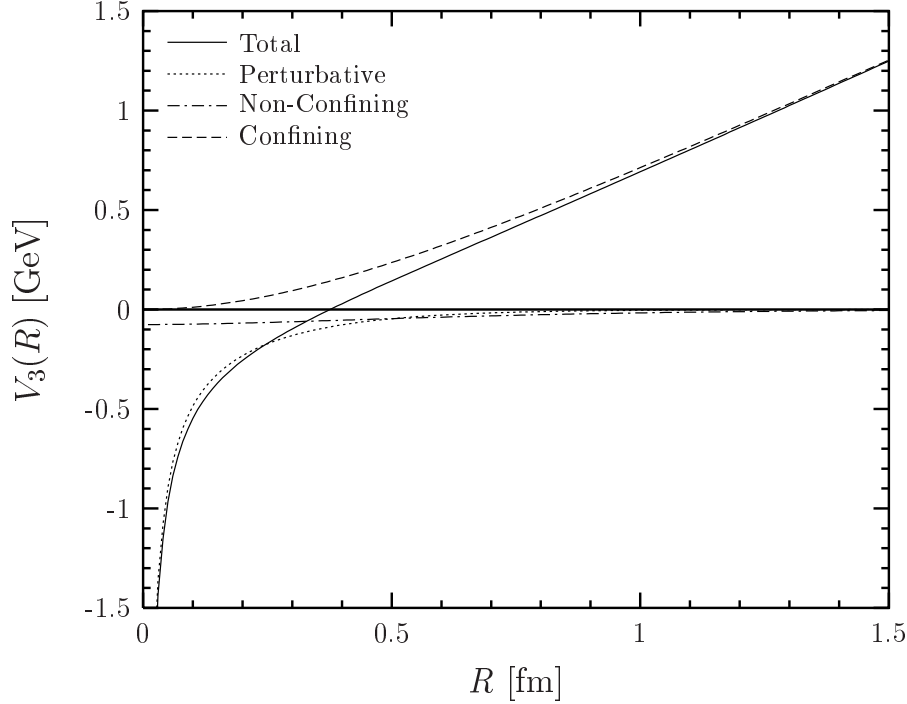


Figure 9: The static $SU(N_c = 3)$ quark-antiquark potential $V_{N_c}(R) = V_3(R)$ as a function of the quark-antiquark separation R . The solid, dotted, and dashed lines indicate the full static potential and its perturbative and non-perturbative contributions, respectively. For small quark-antiquark separations, $R \lesssim 0.5$ fm, the perturbative contribution dominates and gives rise to the well-known color-Coulomb behavior at small distances. For medium and large quark-antiquark separations, $R \gtrsim 0.5$ fm, the non-perturbative contribution dominates and leads to the confining linear rise of the static potential. As our model is working in the quenched approximation, string breaking cannot be described, which is expected to stop the linear increase for $R \gtrsim 1$ fm [50, 75].

0.5 fm, the perturbative contribution dominates giving rise to the well-known color-Coulomb behavior. For medium and large quark-antiquark separations $R \gtrsim 0.5$ fm, the non-perturbative contribution dominates and leads to the confining linear rise of the static potential. The transition from perturbative to string behavior takes place at source separations of about 0.5 fm in agreement with the recent results of Lüscher and Weisz [16]. This supports our value for the gluon mass $m_G = m_\rho = 0.77$ GeV which is only important around $R \approx 0.4$ fm, i.e., for the interplay between the perturbative and non-perturbative physics. For $R \lesssim 0.3$ fm and $R \gtrsim 0.5$ fm, the effect of the gluon mass, introduced as an IR regulator in our perturbative component, is negligible. String breaking is expected to stop the linear increase for $R \gtrsim 1$ fm where lattice investigations show deviations from the linear rise in full QCD [50, 75]. As our model is working in the quenched approximation, string

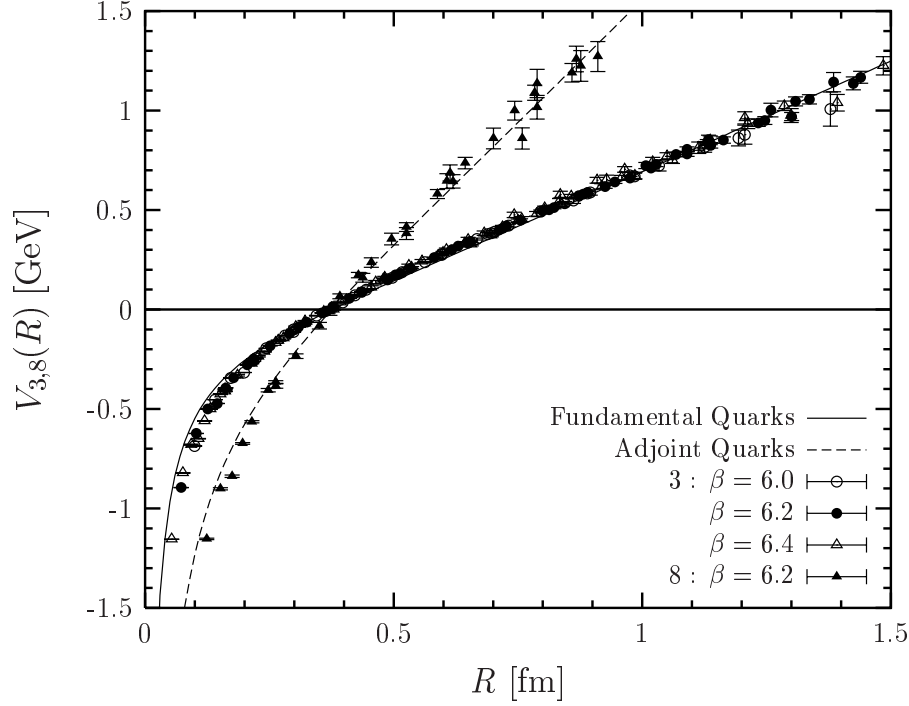


Figure 10: The static $SU(N_c = 3)$ potential of color-dipoles in the fundamental representation $V_3(R)$ (solid line) and adjoint representation $V_8(R)$ (dashed line) as a function of the dipole size R in comparison to $SU(3)$ lattice data for $\beta = 6.0, 6.2$, and 6.4 [50, 55]. The model results are in good agreement with the lattice data. This holds in particular for the obtained Casimir scaling behavior.

breaking through dynamical quark-antiquark production is excluded.

As can be seen from (A.2), the static potential shows *Casimir scaling* which emerges in our approach as a trivial consequence of the Gaussian approximation used to truncate the cumulant expansion (2.7). This is in line with the obtained Casimir scaling of the chromo-electric fields discussed in Sec. 3. In contrast to our model, the instanton model can neither describe Casimir scaling [57] nor the linear rise of the confining potential [76].

Figure 10 shows the static $SU(N_c = 3)$ potential for fundamental sources $V_{N_c}(R) = V_3(R)$ (solid line) and adjoint sources $V_{N_c^2-1}(R) = V_8(R)$ (dashed line) as a function of the dipole size R in comparison to $SU(3)$ lattice data [50, 55]. The model results are in good agreement with the lattice data. In particular, the obtained Casimir scaling behavior is strongly supported by $SU(3)$ lattice data [54, 55]. A shortcoming of our model discussed already in Sec. 3 reappears in the static dipole potential: From Eq. (A.2) and Fig. 10 it is clear that string breaking is neither described for

fundamental nor for adjoint dipoles in our model which indicates again that not only dynamical fermions (quenched approximation) are missing but also some gluon dynamics.

B Loop and Minimal Surface Parametrizations

A rectangular *loop* C_i with “spatial” extension R_i and “temporal” extension T_i placed in four-dimensional Euclidean space — as shown in Fig. 11 — has the following parameter representation

$$C_i = C_i^A \cup C_i^B \cup C_i^C \cup C_i^D \quad (\text{B.1})$$

with

$$C_i^A = \left\{ X_i^A(u_i) = X_{0i} - (1 - z_i) r_i + u_i t_i, \quad u_i \in [-T_i, T_i] \right\} \quad (\text{B.2})$$

$$C_i^B = \left\{ X_i^B(v_i) = X_{0i} - (1 - z_i) r_i + v_i r_i + T_i t_i, \quad v_i \in [0, 1] \right\} \quad (\text{B.3})$$

$$C_i^C = \left\{ X_i^C(u_i) = X_{0i} + z_i r_i + u_i t_i, \quad u_i \in [T_i, -T_i] \right\} \quad (\text{B.4})$$

$$C_i^D = \left\{ X_i^D(v_i) = X_{0i} - (1 - z_i) r_i + v_i r_i + T_i t_i, \quad v_i \in [1, 0] \right\} \quad (\text{B.5})$$

where

$$r_i := \begin{pmatrix} R_i \sin \theta_i \cos \phi_i \\ R_i \sin \theta_i \sin \phi_i \\ R_i \cos \theta_i \cos \Theta_i \\ R_i \cos \theta_i \sin \Theta_i \end{pmatrix} \quad \text{and} \quad t_i := \begin{pmatrix} 0 \\ 0 \\ -\sin \Theta_i \\ \cos \Theta_i \end{pmatrix}. \quad (\text{B.6})$$

The “center” of the loop C_i is given by X_{0i} . The parameters z_i , R_i , θ_i , ϕ_i , and Θ_i are defined in Fig. 11 that illustrates (a) the spatial arrangement of a color-dipole and (b) its world-line C_i in Euclidean “longitudinal” space. The tilting angle $\Theta_i \neq 0$ is the central quantity in the analytic continuation presented in Sec. 5. Moreover, $\Theta_1 = \pi/2$ together with $\Theta_2 = 0$ allows us to compute conveniently the chromomagnetic field distributions in Appendix C.

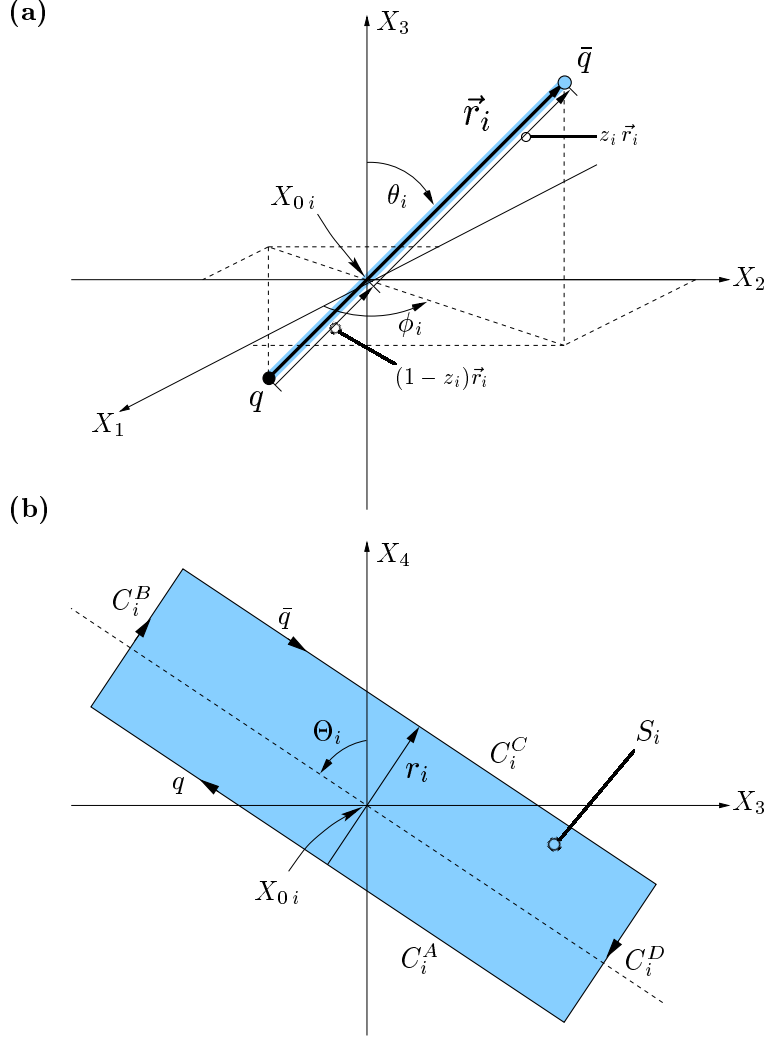


Figure 11: (a) Spatial arrangement of a color-dipole and (b) its world-line in Euclidean “longitudinal” space given by the rectangular *loop* C_i that defines the *minimal surface* S_i with $\partial S_i = C_i$. The minimal surface is represented by the shaded area. In our model, it is interpreted as the world-sheet of the QCD string that confines the quark and antiquark in the dipole.

The *minimal surface* S_i is the planar surface bounded by the loop $C_i = \partial S_i$ given in (B.1). It can be parametrized as follows

$$S_i = \left\{ X_i(u_i, v_i) = X_{0i} - (1 - z_i) r_i + v_i r_i + u_i t_i, \quad u_i \in [-T_i, T_i], \quad v_i \in [0, 1] \right\} \quad (\text{B.7})$$

with r_i and t_i given in (B.6). The corresponding infinitesimal surface element reads

$$d\sigma_{\mu\nu}(X_i) = \left(\frac{\partial X_{i\mu}}{\partial u_i} \frac{\partial X_{i\nu}}{\partial v_i} - \frac{\partial X_{i\mu}}{\partial v_i} \frac{\partial X_{i\nu}}{\partial u_i} \right) du_i dv_i = \left(t_{i\mu} r_{i\nu} - r_{i\mu} t_{i\nu} \right) du_i dv_i. \quad (\text{B.8})$$

C χ -Computations with Minimal Surfaces

The quantities considered in the main text are computed from the VEV of one loop $\langle W[C] \rangle$ and the loop-loop correlation function $\langle W[C_1]W[C_2] \rangle$. Using the Gaussian approximation in the gluon field strengths, both are expressed in terms of $\chi_{S_i S_j}$ -functions (2.15) and (2.27) as shown in Secs. 2.1 and 2.2. These χ -functions are central quantities since here the ansatz of the gauge-invariant bilocal gluon field strength correlator and the surface choice enter the model. In this Appendix, these functions are computed explicitly for minimal surfaces (B.7) and the $F_{\mu\nu\rho\sigma}$ -ansatz given in (2.42), (2.44), and (2.48). Note that the contributions from the infinitesimally thin tube — which allows us to compare the field strengths in surface S_1 with the field strength in surface S_2 — cancel mutually.

Depending on the geometries and the relative arrangement of the loops, the χ -functions determine the physical quantities investigated within the LLCM such as the static $q\bar{q}$ potential (A.2), the chromo-field distributions of a color-dipole (3.9), and the S -matrix element for elastic dipole-dipole scattering (5.10).

We compute separately the three components $\chi_{S_1 S_2}^P$, $\chi_{S_1 S_2}^{NP nc}$, and $\chi_{S_1 S_2}^{NP c}$ for general loop arrangements from which the considered quantities are obtained as special cases. Without loss of generality, the center of the loop C_2 is placed at the origin of the coordinate system, $X_{02} = (0, 0, 0, 0)$. Moreover, C_2 is kept untilted, $\Theta_2 = 0$, and $\Theta := \Theta_1$ is used to simplify notation. We limit our general computation to loops with $r_{1,2} = (\vec{r}_{1,2\perp}, 0, 0) \equiv \theta_{1,2} = \pi/2$ and transverse “impact parameters” $b = X_{01} - X_{02} = X_{01} = (b_1, b_2, 0, 0) = (\vec{b}_\perp, 0, 0)$ which allows to compute all of the considered quantities.

$\chi_{S_1 S_2}^{NPc}$ -Computation

Starting with the definition

$$\begin{aligned}\chi_{S_1 S_2}^{NPc} &:= \frac{\pi^2}{4} \int_{S_1} d\sigma_{\mu\nu}(X_1) \int_{S_2} d\sigma_{\rho\sigma}(X_2) F_{\mu\nu\rho\sigma}^{NPc}(Z = X_1 - X_2) \\ &= \frac{\pi^2 G_2 \kappa}{12(N_c^2 - 1)} \int_{S_1} d\sigma_{\mu\nu}(X_1) \int_{S_2} d\sigma_{\rho\sigma}(X_2) (\delta_{\mu\rho} \delta_{\nu\sigma} - \delta_{\mu\sigma} \delta_{\nu\rho}) D(Z^2),\end{aligned}\quad (C.1)$$

one exploits the anti-symmetry of the surface elements, $d\sigma_{\mu\nu} = -d\sigma_{\nu\mu}$, and applies the surface parametrization (B.7) with the corresponding surface elements (B.8) to obtain

$$\chi_{S_1 S_2}^{NPc} = \cos \Theta \frac{\pi^2 G_2 \kappa}{3(N_c^2 - 1)} (r_1 \cdot r_2) \int_0^1 dv_1 \int_0^1 dv_2 \int_{-T_1}^{T_1} du_1 \int_{-T_2}^{T_2} du_2 D(Z^2) \quad (C.2)$$

with

$$Z = X_1 - X_2 = \begin{pmatrix} \vec{b}_\perp - (1 - z_1) \vec{r}_{1\perp} + v_1 \vec{r}_{1\perp} + (1 - z_2) \vec{r}_{2\perp} - v_2 \vec{r}_{2\perp} \\ -u_1 \sin \Theta \\ u_1 \cos \Theta - u_2 \end{pmatrix}, \quad (C.3)$$

where the identities $t_1 \cdot r_2 = r_1 \cdot t_2 = 0$ and $t_1 \cdot t_2 = \cos \Theta$, evident from (B.6) with the mentioned specification of the loop geometries, have been used. In the limit $T_2 \rightarrow \infty$, the u_2 integration can be performed

$$\begin{aligned}\lim_{T_2 \rightarrow \infty} \int_{-T_2}^{T_2} du_2 D(Z^2) &= \int \frac{d^4 K}{(2\pi)^4} \tilde{D}(K^2) \lim_{T_2 \rightarrow \infty} \int_{-T_2}^{T_2} du_2 e^{iKZ} \\ &= \int \frac{d^4 K}{(2\pi)^4} \tilde{D}(K^2) 2\pi \delta(K_4) \exp[i\vec{K}_\perp \vec{Z}_\perp + iK_3 u_1 \sin \Theta + iK_4 u_1 \cos \Theta] \\ &= \int \frac{d^3 K}{(2\pi)^3} \tilde{D}^{(3)}(\vec{K}^2) \exp[i\vec{K}_\perp \vec{Z}_\perp + iK_3 u_1 \sin \Theta] = D^{(3)}(\vec{Z}^2),\end{aligned}\quad (C.4)$$

which leads to

$$\lim_{T_2 \rightarrow \infty} \chi_{S_1 S_2}^{NPc} = \cos \Theta \frac{\pi^2 G_2 \kappa}{3(N_c^2 - 1)} (\vec{r}_{1\perp} \cdot \vec{r}_{2\perp}) \int_0^1 dv_1 \int_0^1 dv_2 \int_{-T_1}^{T_1} du_1 D^{(3)}(\vec{Z}^2). \quad (C.5)$$

Taking in addition the limit $T_1 \rightarrow \infty$, the u_1 integration can be performed as well

$$\lim_{T_1 \rightarrow \infty} \int_{-T_1}^{T_1} du_1 e^{iK_3 u_1 \sin \Theta} = \begin{cases} 2\pi \delta(K_3 \sin \Theta) = \frac{2\pi \delta(K_3)}{|\sin \Theta|} & \text{for } \sin \Theta \neq 0 \\ \lim_{T_1 \rightarrow \infty} 2T_1 & \text{for } \sin \Theta = 0 \end{cases}. \quad (C.6)$$

With $T_1 = T_2 = T/2 \rightarrow \infty$, one obtains for $\sin \Theta \neq 0$

$$\lim_{T \rightarrow \infty} \chi_{S_1 S_2}^{NPc} = \frac{\cos \Theta}{|\sin \Theta|} \frac{\pi^2 G_2 \kappa}{3(N_c^2 - 1)} (\vec{r}_{1\perp} \cdot \vec{r}_{2\perp}) \int_0^1 dv_1 \int_0^1 dv_2 D^{(2)}(\vec{Z}_\perp^2) \quad (C.7)$$

and for $\sin \Theta = 0$

$$\lim_{T \rightarrow \infty} \chi_{S_1 S_2}^{NPc} = \lim_{T \rightarrow \infty} T \cos \Theta \frac{\pi^2 G_2 \kappa}{3(N_c^2 - 1)} (\vec{r}_{1\perp} \cdot \vec{r}_{2\perp}) \int_0^1 dv_1 \int_0^1 dv_2 D^{(3)}(\vec{Z}^2) . \quad (C.8)$$

Evidently, (C.7) is the result given in (5.12) and (5.15) that describes the confining contribution to the dipole-dipole scattering matrix element S_{DD} .

From (C.8), one obtains the confining contribution to the static color-dipole potential for $S_1 = S_2 = S$ which implies $T_1 = T_2 = T/2$, $\Theta = 0$, $z_1 = z_2$, $r_1 = r_2 = r$, and $\vec{r}_{1\perp} \cdot \vec{r}_{2\perp} = r^2 = R^2$ so that

$$\begin{aligned} \lim_{T \rightarrow \infty} \chi_{SS}^{NPc} &= \lim_{T \rightarrow \infty} T \frac{\pi^2 G_2 \kappa}{3(N_c^2 - 1)} R^2 \int_0^1 dv_1 \int_0^1 dv_2 D^{(3)}(\vec{Z}^2 = (v_1 - v_2)^2 R^2) \\ &= \lim_{T \rightarrow \infty} T \frac{2\pi^2 G_2 \kappa}{3(N_c^2 - 1)} R^2 \int_0^1 d\rho (1 - \rho) D^{(3)}(\rho^2 R^2) , \end{aligned} \quad (C.9)$$

which leads directly to (A.7).

From (C.5) the confining contribution to the chromo-field distributions $\Delta G_{\alpha\beta}^2(X)$ can be computed conveniently. Equation (C.5) reads for $S_1 = S_P$, $T_1 = R_P/2$ and $R_1 = R_P$, and $S_2 = S_W$, $T_2 = T/2$ and $R_2 = R$

$$\lim_{T \rightarrow \infty} \chi_{S_P S_W}^{NPc} = \cos \Theta \frac{\pi^2 G_2 \kappa}{3(N_c^2 - 1)} (\vec{r}_{1\perp} \cdot \vec{r}_{2\perp}) \int_0^1 dv_1 \int_0^1 dv_2 \int_{-R_P/2}^{R_P/2} du_1 D^{(3)}(\vec{Z}^2) \quad (C.10)$$

with

$$\vec{Z} = \vec{X}_1 - \vec{X}_2 = \begin{pmatrix} \vec{b}_\perp - (1 - z_1) \vec{r}_{1\perp} + v_1 \vec{r}_{1\perp} + (1 - z_2) \vec{r}_{2\perp} - v_2 \vec{r}_{2\perp} \\ -u_1 \sin \Theta \end{pmatrix} . \quad (C.11)$$

The confining non-perturbative contribution to the chromo-magnetic fields vanishes as it is obtained for plaquettes with $\Theta = \pi/2$. The corresponding contribution to the chromo-electric fields can be computed with $\Theta = 0$ as follows: Due to $R_1 = R_P \rightarrow 0$, the u_1 and v_1 integrations in (C.10) can be performed with the mean value theorem. Keeping only terms up to $\mathcal{O}(R_p^2)$, the confining non-perturbative contribution to the chromo-field distributions $\Delta G_{\alpha\beta}^2(X)$ is obtained as given in (3.18).

$\chi_{S_1 S_2}^{NP nc}$ -Computation

We start again with the definition

$$\begin{aligned}\chi_{S_1 S_2}^{NP nc} &:= \frac{\pi^2}{4} \int_{S_1} d\sigma_{\mu\nu}(X_1) \int_{S_2} d\sigma_{\rho\sigma}(X_2) F_{\mu\nu\rho\sigma}^{NP nc}(Z = X_1 - X_2) \\ &= \frac{\pi^2 G_2(1-\kappa)}{12(N_c^2 - 1)} \int_{S_1} d\sigma_{\mu\nu}(X_1) \int_{S_2} d\sigma_{\rho\sigma}(X_2) \\ &\quad \times \frac{1}{2} \left[\frac{\partial}{\partial Z_\nu} (Z_\sigma \delta_{\mu\rho} - Z_\rho \delta_{\mu\sigma}) + \frac{\partial}{\partial Z_\mu} (Z_\rho \delta_{\nu\sigma} - Z_\sigma \delta_{\nu\rho}) \right] D_1(Z^2)\end{aligned}\tag{C.12}$$

and use the anti-symmetry of both surface elements to obtain

$$\chi_{S_1 S_2}^{NP nc} = \frac{\pi^2 G_2(1-\kappa)}{6(N_c^2 - 1)} \int_{S_1} d\sigma_{\mu\nu}(X_1) \int_{S_2} d\sigma_{\rho\sigma}(X_2) \frac{\partial}{\partial Z_\nu} Z_\sigma \delta_{\mu\rho} D_1(Z^2) \tag{C.13}$$

$$= \frac{\pi^2 G_2(1-\kappa)}{3(N_c^2 - 1)} \int_{S_1} d\sigma_{\mu\nu}(X_1) \int_{S_2} d\sigma_{\rho\sigma}(X_2) \frac{\partial}{\partial Z_\nu} \frac{\partial}{\partial Z_\sigma} \delta_{\mu\rho} D_1'(Z^2) \tag{C.14}$$

$$= -\frac{\pi^2 G_2(1-\kappa)}{3(N_c^2 - 1)} \int_{S_1} d\sigma_{\mu\nu}(X_1) \frac{\partial}{\partial X_{1\nu}} \int_{S_2} d\sigma_{\rho\sigma}(X_2) \frac{\partial}{\partial X_{2\sigma}} \delta_{\mu\rho} D_1'(Z^2) \tag{C.15}$$

with

$$D_1'(Z^2) = \int \frac{d^4 K}{(2\pi)^4} e^{iKZ} \tilde{D}_1'(K^2) = \int \frac{d^4 K}{(2\pi)^4} e^{iKZ} \frac{d}{dK^2} \tilde{D}_1(K^2) . \tag{C.16}$$

As evident from (C.15), Stokes' theorem can be used to transform each of the surface integrals in $\chi_{S_1 S_2}^{NP nc}$ into a line integral

$$\chi_{S_1 S_2}^{NP nc} = -\frac{\pi^2 G_2(1-\kappa)}{3(N_c^2 - 1)} \int_{S_1} d\sigma_{\mu\nu}(X_1) \frac{\partial}{\partial Z_\nu} \oint_{C_2} dZ_\rho(X_2) \delta_{\mu\rho} D_1'(Z^2) \tag{C.17}$$

$$= -\frac{\pi^2 G_2(1-\kappa)}{6(N_c^2 - 1)} \int_{S_1} d\sigma_{\mu\nu}(X_1) \oint_{C_2} dZ_\rho(X_2) \delta_{\mu\rho} Z_\nu D_1(Z^2) \tag{C.18}$$

$$= -\frac{\pi^2 G_2(1-\kappa)}{3(N_c^2 - 1)} \oint_{C_1} dZ_\mu(X_1) \oint_{C_2} dZ_\rho(X_2) \delta_{\mu\rho} D_1'(Z^2) . \tag{C.19}$$

With the line parametrizations of C_1 and C_2 given in (B.1) and the specification of the loop geometries mentioned at the beginning of this appendix, (C.19) becomes

$$\begin{aligned}\chi_{S_1 S_2}^{NP nc} &= -\frac{\pi^2 G_2(1-\kappa)}{3(N_c^2 - 1)} \\ &\times \left\{ \cos \Theta \int_{-T_1}^{T_1} du_1 \int_{-T_2}^{T_2} du_2 \left[D_1'(Z_{AA}^2) - D_1'(Z_{AC}^2) - D_1'(Z_{CA}^2) + D_1'(Z_{CC}^2) \right] \right. \\ &\quad \left. + (\vec{r}_{1\perp} \cdot \vec{r}_{2\perp}) \int_0^1 dv_1 \int_0^1 dv_2 \left[D_1'(Z_{BB}^2) - D_1'(Z_{BD}^2) - D_1'(Z_{DB}^2) + D_1'(Z_{DD}^2) \right] \right\}\end{aligned}\tag{C.20}$$

where the following shorthand notation is used

$$Z_{XY} := X_1^X - X_2^Y \quad \text{with} \quad X_2^X \in C_2^X \quad \text{and} \quad X_2^Y \in C_2^Y. \quad (\text{C.21})$$

In the limit $R_{1,2} \ll T_{1,2} \rightarrow \infty$, the term $\propto (\vec{r}_{1\perp} \cdot \vec{r}_{2\perp})$ on the rhs of (C.20) can be neglected and, thus, (C.20) reduces to

$$\begin{aligned} \lim_{\substack{T_1 \rightarrow \infty \\ T_2 \rightarrow \infty}} \chi_{S_1 S_2}^{NPnc} = & -\cos \Theta \frac{\pi^2 G_2 (1 - \kappa)}{3(N_c^2 - 1)} \lim_{T_1 \rightarrow \infty} \int_{-T_1}^{T_1} du_1 \lim_{T_2 \rightarrow \infty} \int_{-T_2}^{T_2} du_2 \quad (\text{C.22}) \\ & \times \left[D'_1(Z_{AA}^2) - D'_1(Z_{AC}^2) - D'_1(Z_{CA}^2) + D'_1(Z_{CC}^2) \right]. \end{aligned}$$

Here, the integrations over u_1 and u_2 can be performed analytically proceeding analogously to (C.4) and (C.6). With $T_1 = T_2 = T/2 \rightarrow \infty$, one obtains for $\sin \Theta \neq 0$

$$\begin{aligned} \lim_{T \rightarrow \infty} \chi_{S_1 S_2}^{NPnc} = & -\frac{\cos \Theta}{|\sin \Theta|} \frac{\pi^2 G_2 (1 - \kappa)}{3(N_c^2 - 1)} \quad (\text{C.23}) \\ & \times \left[D_1'^{(2)}(\vec{Z}_{AA\perp}^2) - D_1'^{(2)}(\vec{Z}_{AC\perp}^2) - D_1'^{(2)}(\vec{Z}_{CA\perp}^2) + D_1'^{(2)}(\vec{Z}_{CC\perp}^2) \right] \end{aligned}$$

and for $\sin \Theta = 0$

$$\begin{aligned} \lim_{T \rightarrow \infty} \chi_{S_1 S_2}^{NPnc} = & -\lim_{T \rightarrow \infty} T \cos \Theta \frac{\pi^2 G_2 (1 - \kappa)}{3(N_c^2 - 1)} \quad (\text{C.24}) \\ & \times \left[D_1'^{(3)}(\vec{Z}_{AA}^2) - D_1'^{(3)}(\vec{Z}_{AC}^2) - D_1'^{(3)}(\vec{Z}_{CA}^2) + D_1'^{(3)}(\vec{Z}_{CC}^2) \right]. \end{aligned}$$

With the following identities

$$\vec{Z}_{AA\perp} = \vec{r}_{1q} - \vec{r}_{2q}, \quad \vec{Z}_{AC\perp} = \vec{r}_{1q} - \vec{r}_{2\bar{q}}, \quad \vec{Z}_{CA\perp} = \vec{r}_{1\bar{q}} - \vec{r}_{2q}, \quad \vec{Z}_{CC\perp} = \vec{r}_{1\bar{q}} - \vec{r}_{2\bar{q}}, \quad (\text{C.25})$$

one sees immediately that (C.23) is the result given in (5.12) and (5.14) that describes the non-confining non-perturbative contribution to the dipole-dipole scattering matrix element S_{DD} .

From (C.24), one obtains the non-confining contribution to the static potential for $S_1 = S_2 = S$, i.e., $T_1 = T_2 = T/2$, $\Theta = 0$, $r_1 = r_2 = r$,

$$\begin{aligned} \lim_{T \rightarrow \infty} \chi_{SS}^{NPnc} = & -\lim_{T \rightarrow \infty} T \frac{\pi^2 G_2 (1 - \kappa)}{3(N_c^2 - 1)} \quad (\text{C.26}) \\ & \times \left[D_1'^{(3)}(\vec{Z}_{AA}^2) - D_1'^{(3)}(\vec{Z}_{AC}^2) - D_1'^{(3)}(\vec{Z}_{CA}^2) + D_1'^{(3)}(\vec{Z}_{CC}^2) \right], \end{aligned}$$

which contributes to the self-energy of the color-sources with

$$\begin{aligned}\lim_{T \rightarrow \infty} \chi_{SS \text{ self}}^{NP nc} &= - \lim_{T \rightarrow \infty} T \frac{\pi^2 G_2 (1 - \kappa)}{3(N_c^2 - 1)} \left[D_1'^{(3)}(\vec{Z}_{AA}^2) + D_1'^{(3)}(\vec{Z}_{CC}^2) \right] \\ &= - \lim_{T \rightarrow \infty} T \frac{2\pi^2 G_2 (1 - \kappa)}{3(N_c^2 - 1)} D_1'^{(3)}(\vec{Z}_{AA}^2)\end{aligned}\quad (\text{C.27})$$

and to the potential energy between the color-sources with

$$\begin{aligned}\lim_{T \rightarrow \infty} \chi_{SS \text{ pot}}^{NP nc} &= \lim_{T \rightarrow \infty} T \frac{\pi^2 G_2 (1 - \kappa)}{6(N_c^2 - 1)} \left[D_1'^{(3)}(\vec{Z}_{AC}^2) + D_1'^{(3)}(\vec{Z}_{CA}^2) \right] \\ &= \lim_{T \rightarrow \infty} T \frac{\pi^2 G_2 (1 - \kappa)}{3(N_c^2 - 1)} D_1'^{(3)}(\vec{Z}_{AC}^2) .\end{aligned}\quad (\text{C.28})$$

The latter gives the non-confining contribution to the static potential (A.6).

The non-confining non-perturbative contribution to the chromo-electric fields ($\Delta G_{\alpha\beta}^2(X)$ with $\alpha\beta = i4 = 4i$) can be computed most conveniently from (C.18) with zero plaquette tilting angle $\Theta = 0$. The corresponding contribution to the chromo-magnetic fields ($\Delta G_{\alpha\beta}^2(X)$ with $\alpha\beta = ij = ji$) is obtained for plaquette tilting angle $\Theta = \pi/2$ and thus vanishes which can be seen most directly from the surface integrals (C.13). Now, we set $\Theta = 0$ to compute the contribution to the chromo-electric fields: Using the surface $S_1 = S_P$ and loop $C_2 = \partial S_W$ parametrizations, (B.7) and (B.1), with our specification of the loop geometries, one obtains from (C.18)

$$\begin{aligned}\chi_{S_P S_W}^{NP nc} &= - \frac{\pi^2 G_2 (1 - \kappa)}{3(N_c^2 - 1)} \int_{-R_P/2}^{R_P/2} du_1 \int_0^1 dv_1 \\ &\times \left\{ \int_{-T/2}^{T/2} du_2 \left[(\vec{r}_{1\perp} \cdot \vec{Z}_{1A\perp}) D_1(Z_{1A}^2) - (\vec{r}_{1\perp} \cdot \vec{Z}_{1C\perp}) D_1(Z_{1C}^2) \right] \right. \\ &\quad \left. - (\vec{r}_{1\perp} \cdot \vec{r}_{2\perp}) \int_0^1 dv_2 \left[(\vec{r}_{1\perp} \cdot \vec{Z}_{1B\perp}) D_1(Z_{1B}^2) - (\vec{r}_{1\perp} \cdot \vec{Z}_{1D\perp}) D_1(Z_{1D}^2) \right] \right\}\end{aligned}\quad (\text{C.29})$$

with $T_1 = R_P/2$, $R_1 = R_P$, $T_2 = T/2$, $R_2 = R$, and the shorthand notation

$$Z_{1X} := X_1 - X_2^X \quad \text{with} \quad X_1 \in S_1 = S_P \quad \text{and} \quad X_2^X \in C_2^X = \partial S_W^X . \quad (\text{C.30})$$

In the limit $R \ll T \rightarrow \infty$, the term $\propto (\vec{r}_{1\perp} \cdot \vec{r}_{2\perp})$ on the rhs of (C.29) can be neglected

$$\begin{aligned}\lim_{T \rightarrow \infty} \chi_{S_P S_W}^{NP nc} &= - \frac{\pi^2 G_2 (1 - \kappa)}{3(N_c^2 - 1)} \int_{-R_P/2}^{R_P/2} du_1 \int_0^1 dv_1 \lim_{T \rightarrow \infty} \int_{-T/2}^{T/2} du_2 \\ &\times \left[(\vec{r}_{1\perp} \cdot \vec{Z}_{1A\perp}) D_1(Z_{1A}^2) - (\vec{r}_{1\perp} \cdot \vec{Z}_{1C\perp}) D_1(Z_{1C}^2) \right] .\end{aligned}\quad (\text{C.31})$$

With an infinitesimal plaquette used to measure the chromo-electric field, $R_1 = R_p \rightarrow 0$, the mean value theorem can be used to perform the u_1 and v_1 integrations in (C.31). Keeping only terms up to $\mathcal{O}(R_p^2)$, this leads directly to the non-confining non-perturbative contribution to the chromo-field distributions $\Delta G_{\alpha\beta}^2(X)$ as given in (3.16) and (3.17).

χ^P -Computation

Comparing the definition of the perturbative component

$$\begin{aligned}\chi_{S_1 S_2}^P &:= \frac{\pi^2}{4} \int_{S_1} d\sigma_{\mu\nu}(X_1) \int_{S_2} d\sigma_{\rho\sigma}(X_2) F_{\mu\nu\rho\sigma}^P(Z = X_1 - X_2) \\ &= \frac{g^2}{4} \int_{S_1} d\sigma_{\mu\nu}(X_1) \int_{S_2} d\sigma_{\rho\sigma}(X_2) \\ &\quad \times \frac{1}{2} \left[\frac{\partial}{\partial Z_\nu} (Z_\sigma \delta_{\mu\rho} - Z_\rho \delta_{\mu\sigma}) + \frac{\partial}{\partial Z_\mu} (Z_\rho \delta_{\nu\sigma} - Z_\sigma \delta_{\nu\rho}) \right] D_P(Z^2)\end{aligned}\tag{C.32}$$

with the one of the non-confining non-perturbative component $\chi_{S_1 S_2}^{NP\,nc}$ given in (C.12), one finds an identical structure. Thus, accounting for the different prefactors and the different correlation function, the results for $\chi_{S_1 S_2}^P$ can be read off directly from the results for $\chi_{S_1 S_2}^{NP\,nc}$ given above:

With $T_1 = T_2 = T/2 \rightarrow \infty$ and our specification of the loop geometries, one obtains the result for $\sin \Theta \neq 0$ from (C.23)

$$\begin{aligned}\lim_{T \rightarrow \infty} \chi_{S_1 S_2}^P &= - \frac{\cos \Theta}{|\sin \Theta|} g^2 \\ &\quad \times \left[D_P'^{(2)}(\vec{Z}_{AA\perp}^2) - D_P'^{(2)}(Z_{AC\perp}^2) - D_P'^{(2)}(\vec{Z}_{CA\perp}^2) + D_P'^{(2)}(\vec{Z}_{CC\perp}^2) \right]\end{aligned}\tag{C.33}$$

and the result for $\sin \Theta = 0$ from (C.24)

$$\begin{aligned}\lim_{T \rightarrow \infty} \chi_{S_1 S_2}^P &= - \lim_{T \rightarrow \infty} T \cos \Theta g^2 \\ &\quad \times \left[D_P'^{(3)}(\vec{Z}_{AA}^2) - D_P'^{(3)}(Z_{AC}^2) - D_P'^{(3)}(\vec{Z}_{CA}^2) + D_P'^{(3)}(\vec{Z}_{CC}^2) \right],\end{aligned}\tag{C.34}$$

where Z_{XY} is defined in (C.21) and $Z_{XY\perp}$ is given explicitly in (C.25). Evidently, (C.33) is the final result given in (5.12) and (5.13) that describes the perturbative contribution the dipole-dipole scattering matrix element S_{DD} .

The perturbative contribution to the static potential is obtained from the expression corresponding to (C.26),

$$\begin{aligned} \lim_{T \rightarrow \infty} \chi_{SS}^P &= - \lim_{T \rightarrow \infty} T g^2 \\ &\times \left[D_P'^{(3)}(\vec{Z}_{AA}^2) - D_P'^{(3)}(Z_{AC}^2) - D_P'^{(3)}(\vec{Z}_{CA}^2) + D_P'^{(3)}(\vec{Z}_{CC}^2) \right], \end{aligned} \quad (\text{C.35})$$

which contributes to the self-energy of the color-sources with

$$\begin{aligned} \lim_{T \rightarrow \infty} \chi_{SS}^P \text{self} &= - \lim_{T \rightarrow \infty} T g^2 \left[D_P'^{(3)}(\vec{Z}_{AA}^2) + D_P'^{(3)}(\vec{Z}_{CC}^2) \right] \\ &= - \lim_{T \rightarrow \infty} T 2 g^2 D_P'^{(3)}(\vec{Z}_{AA}^2) \end{aligned} \quad (\text{C.36})$$

and to the potential energy between the color-sources with

$$\begin{aligned} \lim_{T \rightarrow \infty} \chi_{SS}^P \text{pot} &= - \lim_{T \rightarrow \infty} T g^2 \left[D_P'^{(3)}(\vec{Z}_{AC}^2) + D_P'^{(3)}(\vec{Z}_{CA}^2) \right] \\ &= - \lim_{T \rightarrow \infty} T 2 g^2 D_P'^{(3)}(\vec{Z}_{AC}^2). \end{aligned} \quad (\text{C.37})$$

The latter gives the perturbative contribution to the static potential (A.4).

The perturbative contribution to the chromo-magnetic fields ($\Delta G_{\alpha\beta}^2(X)$ with $\alpha\beta = ij = ji$) vanishes while the one to the chromo-electric fields ($\Delta G_{\alpha\beta}^2(X)$ with $\alpha\beta = i4 = 4i$) for which a plaquette with $\Theta = 0$ is needed, is obtained from the expression corresponding to (C.31),

$$\begin{aligned} \lim_{T \rightarrow \infty} \chi_{SPSW}^P &= - g^2 \int_{-R_P/2}^{R_P/2} du_1 \int_0^1 dv_1 \lim_{T \rightarrow \infty} \int_{-T/2}^{T/2} du_2 \\ &\times \left[(\vec{r}_{1\perp} \cdot \vec{Z}_{1A\perp}) D_P(Z_{1A}^2) - (\vec{r}_{1\perp} \cdot \vec{Z}_{1C\perp}) D_P(Z_{1C}^2) \right] \end{aligned} \quad (\text{C.38})$$

with Z_{1X} as defined in (C.30). To perform the u_1 and v_1 integrations in (C.38), again the mean value theorem can be used since the plaquette has infinitesimally small extensions, $R_1 = R_p \rightarrow 0$. Keeping only terms up to $\mathcal{O}(R_p^2)$, this leads directly to the perturbative contribution to the chromo-field distribution $\Delta G_{\alpha\beta}^2(X)$ as given in (3.13) and (3.14).

References

- [1] A. Smilga, “Lectures On Quantum Chromodynamics,” (World Scientific, Singapore, 2001).

- [2] A. Ringwald, “Vacuum structure and high-energy scattering,” hep-ph/0210209.
- [3] H. J. Rothe, “Lattice gauge theories: An Introduction,” World Sci. Lect. Notes Phys. **59** (1997) 1.
- [4] A. I. Shoshi, F. D. Steffen and H. J. Pirner, Nucl. Phys. A **709** (2002) 131.
- [5] O. Nachtmann, Annals Phys. **209** (1991) 436;
H. Verlinde and E. Verlinde, “QCD at high-energies and two-dimensional field theory,” hep-th/9302104;
G. P. Korchemsky, Phys. Lett. B **325** (1994) 459.
- [6] O. Nachtmann, in “Perturbative and Nonperturbative Aspects of Quantum Field Theory”, edited by H. Latal and W. Schweiger (Springer Verlag, Berlin, Heidelberg 1997) [hep-ph/9609365].
- [7] A. Krämer and H. G. Dosch, Phys. Lett. B **252** (1990) 669.
- [8] H. G. Dosch, E. Ferreira and A. Krämer, Phys. Rev. D **50** (1994) 1992.
- [9] H. G. Dosch, in “Hadron Physics 96,” edited by E. Ferreira et al., (World Scientific, Singapore 1997).
- [10] F. J. Wegner, J. Math. Phys. **12** (1971) 2259.
- [11] K. G. Wilson, Phys. Rev. D **10** (1974) 2445.
- [12] H. G. Dosch, Phys. Lett. B **190** (1987) 177;
H. G. Dosch and Y. A. Simonov, Phys. Lett. B **205** (1988) 339.
- [13] A. Di Giacomo and H. Panagopoulos, Phys. Lett. B **285** (1992) 133;
A. Di Giacomo, E. Meggiolaro and H. Panagopoulos, Nucl. Phys. B **483** (1997) 371;
M. D’Elia, A. Di Giacomo and E. Meggiolaro, Phys. Lett. B **408** (1997) 315;
G. S. Bali, N. Brambilla and A. Vairo, Phys. Lett. B **421** (1998) 265.
- [14] E. Meggiolaro, Phys. Lett. B **451** (1999) 414.
- [15] M. Rueter and H. G. Dosch, Z. Phys. C **66** (1995) 245.
- [16] M. Lüscher and P. Weisz, JHEP **0207** (2002) 049.
- [17] C. Michael, Nucl. Phys. B **280** (1987) 13.
- [18] H. J. Rothe, Phys. Lett. B **355** (1995) 260; Phys. Lett. B **364** (1995) 227.
- [19] C. Michael, Phys. Rev. D **53** (1996) 4102.

- [20] A. M. Green, C. Michael and P. S. Spencer, Phys. Rev. D **55** (1997) 1216.
- [21] H. G. Dosch, O. Nachtmann and M. Rueter, “String formation in the model of the stochastic vacuum and consistency with low-energy theorems,” hep-ph/9503386.
- [22] A. I. Shoshi, F. D. Steffen and H. J. Pirner, “Gluon Saturation and S-Matrix Unitarity,” hep-ph/0205343.
- [23] A. I. Shoshi, F. D. Steffen, H. G. Dosch and H. J. Pirner, “Decomposition of the QCD String into Dipoles and Unintegrated Gluon Distributions,” hep-ph/0207287.
- [24] E. Meggiolaro, Z. Phys. C **76** (1997) 523; Eur. Phys. J. C **4** (1998) 101; Nucl. Phys. B **625** (2002) 312.
- [25] R. A. Janik and R. Peschanski, Nucl. Phys. B **565** (2000) 193;
R. A. Janik, Acta Phys. Polon. B **32** (2001) 4105.
- [26] M. Rho, S. J. Sin and I. Zahed, Phys. Lett. B **466** (1999) 199.
- [27] E. V. Shuryak and I. Zahed, Phys. Rev. D **62** (2000) 085014;
M. A. Nowak, E. V. Shuryak and I. Zahed, Phys. Rev. D **64** (2001) 034008.
- [28] A. Di Giacomo and E. Meggiolaro, private communication (2002).
- [29] M. Rueter and H. G. Dosch, Phys. Lett. B **380** (1996) 177;
H. G. Dosch, T. Gousset and H. J. Pirner, Phys. Rev. D **57** (1998) 1666;
M. Rueter and H. G. Dosch, Phys. Rev. D **57** (1998) 4097;
G. Kulzinger, H. G. Dosch and H. J. Pirner, Eur. Phys. J. C **7** (1999) 73;
M. Rueter, Eur. Phys. J. C **7** (1999) 233;
U. D’Alesio, A. Metz and H. J. Pirner, Eur. Phys. J. C **9** (1999) 601.
- [30] H. G. Dosch, T. Gousset, G. Kulzinger and H. J. Pirner, Phys. Rev. D **55** (1997) 2602.
- [31] E. R. Berger and O. Nachtmann, Eur. Phys. J. C **7** (1999) 459.
- [32] H. G. Dosch, O. Nachtmann, T. Paulus and S. Weinstock, Eur. Phys. J. C **21** (2001) 339.
- [33] G. Kulzinger, “High-energy scattering in the nonperturbative vacuum of quantum chromodynamics. (In German),” hep-ph/0202125.
- [34] A. Donnachie, H. G. Dosch and M. Rueter, Eur. Phys. J. C **13** (2000) 141;
A. Donnachie and H. G. Dosch, Phys. Rev. D **65** (2002) 014019.

- [35] A. A. Migdal, Phys. Rept. **102** (1983) 199.
- [36] I. Arefeva, Theor. Math. Phys. **43** (1980) 353;
N. E. Bralic, Phys. Rev. D **22** (1980) 3090;
P. M. Fishbane, S. Gasiorowicz and P. Kaus, Phys. Rev. D **24** (1981) 2324;
L. Diosi, Phys. Rev. D **27** (1983) 2552;
Y. A. Simonov, Sov. J. Nucl. Phys. **48** (1988) 878.
- [37] N. G. Van Kampen, Physica **74** (1997) 215, 239; Phys. Rep. **C24** (1976) 172;
A. Y. Dubin and Y. S. Kalashnikova, Phys. Atom. Nucl. **58** (1995) 1967 [Yad. Fiz. **58** (1995) 2078].
- [38] A. Di Giacomo, H. G. Dosch, V. I. Shevchenko and Y. A. Simonov, “Field correlators in QCD: Theory and applications,” hep-ph/0007223.
- [39] P. Cvitanovic, “Group Theory, part I,” Nordita Classics Illustrated (1984); see also <http://www.nbi.dk/GroupTheory/Welcome.html>.
- [40] J. Häkkinen and H. Kharraziha, Comput. Phys. Commun. **100** (1997) 311 [arXiv:hep-ph/9603229].
- [41] V. I. Shevchenko and Y. A. Simonov, Phys. Rev. D **66** (2002) 056012.
- [42] Y. A. Simonov, Phys. Atom. Nucl. **58** (1995) 107.
- [43] V. I. Shevchenko and Y. A. Simonov, Phys. Lett. B **437** (1998) 131.
- [44] M. Eidemüller and M. Jamin, Phys. Lett. B **416** (1998) 415.
- [45] A. Di Giacomo and E. Meggiolaro, Phys. Lett. B **537** (2002) 173.
- [46] M. A. Shifman, A. I. Vainshtein and V. I. Zakharov, Nucl. Phys. B **147** (1979) 385; Nucl. Phys. B **147** (1979) 448.
- [47] H. G. Dosch, M. Eidemüller and M. Jamin, Phys. Lett. B **452** (1999) 379.
- [48] For a review on heavy quarkonium phenomenology, see e.g. W. Kwong, J. L. Rosner and C. Quigg, Ann. Rev. Nucl. Part. Sci. **37** (1987) 325.
- [49] P. Goddard, J. Goldstone, C. Rebbi and C. B. Thorn, Nucl. Phys. B **56** (1973) 109; K. Johnson and C. B. Thorn, Phys. Rev. D **13** (1976) 1934.
- [50] G. S. Bali, Phys. Rept. **343** (2001) 1.
- [51] M. Fukugita and T. Niuya, Phys. Lett. B **132** (1983) 374.
- [52] J. W. Flower and S. W. Otto, Phys. Lett. B **160** (1985) 128.

- [53] J. Ambjorn, P. Olesen and C. Peterson, Nucl. Phys. B **240** (1984) 533.
- [54] S. Deldar, Phys. Rev. D **62** (2000) 034509.
- [55] G. S. Bali, Phys. Rev. D **62** (2000) 114503.
- [56] V. I. Shevchenko and Y. A. Simonov, Phys. Rev. Lett. **85** (2000) 1811.
- [57] V. I. Shevchenko and Y. A. Simonov, “On Casimir Scaling in QCD,” hep-ph/0104135.
- [58] H. D. Trottier, Phys. Lett. B **357** (1995) 193.
- [59] K. Kallio and H. D. Trottier, “Adjoint ‘quarks’ on coarse anisotropic lattices: Implications for string breaking in full QCD,” hep-lat/0001020.
- [60] S. Gusken, Nucl. Phys. Proc. Suppl. **63** (1998) 16;
S. Aoki *et al.* [CP-PACS Collaboration], Nucl. Phys. Proc. Suppl. **73** (1999) 216.
- [61] S. Mandelstam, Phys. Rept. **23** (1976) 245;
G. ’t Hooft, in Proc. Int. School of Subnuclear Physics, Erice, Jul 11-31, 1975, ed. A. Zichichi (Plenum Press, New York, 1977); Nucl. Phys. B **190** (1981) 455.
- [62] M. Baker, J. S. Ball and F. Zachariasen, Phys. Rept. **209** (1991) 73.
- [63] M. Baker, N. Brambilla, H. G. Dosch and A. Vairo, Phys. Rev. D **58** (1998) 034010.
- [64] G. S. Bali, K. Schilling and C. Schlichter, Phys. Rev. D **51** (1995) 5165.
- [65] V. A. Novikov, M. A. Shifman, A. I. Vainshtein and V. I. Zakharov, Nucl. Phys. B **191** (1981) 301; Sov. J. Part. Nucl. **13** (1982) 224.
- [66] L. S. Brown and W. I. Weisberger, Phys. Rev. D **20** (1979) 3239.
- [67] X. D. Ji, Phys. Rev. D **52** (1995) 271.
- [68] F. E. Low, Phys. Rev. D **12** (1975) 163;
S. Nussinov, Phys. Rev. Lett. **34** (1975) 1286.
- [69] J. F. Gunion and D. E. Soper, Phys. Rev. D **15** (1977) 2617.
- [70] T. Appelquist and W. Fischler, Phys. Lett. B **77** (1978) 405.
- [71] G. Bhanot, W. Fischler and S. Rudaz, Nucl. Phys. B **155** (1979) 208.

- [72] M. E. Peskin, Nucl. Phys. B **156** (1979) 365;
G. Bhanot and M. E. Peskin, Nucl. Phys. B **156** (1979) 391.
- [73] A. Hebecker, E. Meggiolaro and O. Nachtmann, Nucl. Phys. B **571** (2000) 26;
O. Nachtmann, “Effective field theory approach to structure functions at small $x(Bj)$,” hep-ph/0206284.
- [74] H. J. Pirner, Phys. Lett. B **521** (2001) 279;
H. J. Pirner and F. Yuan, Phys. Rev. D **66** (2002) 034020.
- [75] E. Laermann, C. DeTar, O. Kaczmarek and F. Karsch, Nucl. Phys. Proc. Suppl. **73** (1999) 447.
- [76] D. Chen, R. C. Brower, J. W. Negele and E. V. Shuryak, Nucl. Phys. Proc. Suppl. **73** (1999) 512.